NACA

RESEARCH MEMORANDUM

THE EFFECT OF THE INLET MACH NUMBER AND INLET-BOUNDARY-

LAYER THICKNESS ON THE PERFORMANCE OF A 23° CONICAL-

DIFFUSER - TAIL-PIPE COMBINATION

By Jerome Persh

Langley Aeronautical Laboratory
Langley Air Force Base, Va.

NATIONAL ADVISORY COMMITTEE
FOR AERONAUTICS

WASHINGTON

March 21, 1950

NATIONAL ADVISORY COMMITTEE FOR AERONAUTICS

RESEARCH MEMORANDUM

THE EFFECT OF THE INLET MACH NUMBER AND INLET-BOUNDARY-

LAYER THICKNESS ON THE PERFORMANCE OF A 23° CONICAL-

DIFFUSER – TAIL-PIPE COMBINATION

By Jerome Persh

SUMMARY

An investigation was conducted to determine the effect of the inlet Mach number and entrance-boundary-layer thickness on the performance of a 23° 21-inch conical-diffuser – tail-pipe combination with a 2:1 area ratio. The air flows used in this investigation covered an inlet Mach number range from 0.17 to 0.89 and corresponding Reynolds numbers of 1,700,000 to 7,070,000. Results are reported for two inlet-boundary-layer thicknesses. Over the entire range of flows, the mean value of the inlet displacement thickness is about 0.034 inch for the thinner inlet boundary layer and about 0.170 inch for the case of the thicker inlet boundary layer.

The performance of the diffuser – tail-pipe combination is presented together with examples of longitudinal static-pressure distribution and the results of boundary-layer pressure surveys made at six points along the diffuser wall.

The results indicated a progressive diminution of the static-pressure recovery and a steady increase in the total-pressure losses as the inlet Mach number was increased for both inlet-boundary-layer thicknesses. The ratio of actual static-pressure rise to that theoretically possible was much less and the total-pressure losses were greater for the case of the thicker inlet boundary layer throughout the speed range investigated. With the thinner inlet boundary layer, flow separation occurred at the diffuser exit at all inlet Mach numbers. Unseparated flow alternating with separated flow was observed near the inlet at the higher velocities. For the case of the thicker inlet boundary layer, the origin of the separated region occurred in the vicinity of the inlet-duct-diffuser junction section at all Mach numbers.

INTRODUCTION

Although previous research has associated the inefficiency of wide-
angle diffusers with separation of the boundary layer, little is known
of the mechanism of the diffusion process and its relationship to the
characteristics of the boundary layer. Furthermore, the results of
previous investigations are inapplicable to the design of modern aircraft
duct systems because the air-flow rates at which these investigations
have been conducted did not incorporate the combination of large Reynolds
numbers at high-subsonic Mach numbers which are common to present-day
aircraft.

Among the earliest available data relating to the subject of diffusers
were those presented by Gibson (reference 1) who sought to determine the
relationship between the energy loss and the included angle of diffusers
with a constant area ratio of 4:1. Later research by Peters (reference 2)
was undertaken to determine the influence on the diffuser efficiency of
systematically varying the initial velocity profile. The area ratio of
the diffusers used in his experiments was 2.34:1. Early research by
Kröner (reference 3) was undertaken to investigate the separation phenomena
and the relationship to the energy losses in wide-angle, two-dimensional
diffusers of area ratio 14.3:1. It was found in these experiments that
boundary-layer separation (observed when the total included angle was
increased beyond 12°) produced different results for each successive test,
and it was not possible to draw any definite conclusions beyond the point
at which separation becomes perceptible. It was found experimentally
by Vedernikoff (reference 4) that separation first occurred at a total
included angle of about 14°. In these tests the length of the diffuser
was kept constant, the area ratio being varied with angle. In his tests
of diffusers with total included angles greater than 14°, the flow
appeared to be nonuniform and the losses increased considerably.

In an attempt to obtain a better understanding of the mechanism of
diffuser flow over a range of speeds of interest in aircraft design, a
systematic series of investigations was undertaken in which the flow in
conical diffusers varying in size and divergence angle was measured.
For all experiments the area ratio was held constant. Particular emphasis
was put on the boundary-layer growth and its relationship to performance.
Some of the initial results obtained with a 12° 21-inch conical diffuser,
having a 2:1 area ratio, with varying inlet-boundary-layer thickness are
reported in reference 5. The present paper is a continuation of this
investigation using a diffuser of the same size, with an arbitrarily
chosen included angle large enough to induce boundary-layer separation.
For these experiments a tail pipe of constant diameter was used following
the diffuser as an experimental tool for obtaining adequate pressure
measurements. By this procedure, the specific case of a conical expansion

followed by a straight duct is investigated. This configuration is
treated as a whole because of the inseparable interrelation between the
two duct components.

It is the purpose of the present experimental investigation to provide
flow data obtained in tests of a 23° 21-inch conical-diffuser — tail-pipe
combination with a 2:1 area ratio, under two different inlet-boundary-layer
conditions. The constant-area tail pipe used was about $3\frac{1}{2}$ inlet diameters
in length. The data presented herein cover an inlet Mach number range
from 0.17 to 0.89 corresponding to Reynolds numbers of 1,700,000 to
7,070,000, based on inlet diameter. Pressure measurements were made
from which the over-all performance of the diffuser, the longitudinal
variation in static pressure, and the boundary-layer characteristics are
determined. Explanations of the interrelation of the performance results
and the boundary-layer characteristics are given.

SYMBOLS

p static pressure

H total pressure

T total temperature, $^\circ R$

ρ mass density

F_c compressibility factor

R gas constant

γ ratio of specific heats

q_c impact pressure $(H - p)$

ΔH weighted total-pressure loss from mass-flow surveys $\left(H_1 - H_7\right)$

Δp static-pressure rise measured at wall $\left(p_1 - p_6\right)$ and $\left(p_1 - p_7\right)$

Δq_c change in impact pressure $\left(q_{c_1} - q_{c_7}\right)$

r radius

x   distance along longitudinal axis

y   perpendicular distance from diffuser wall

u   local velocity within boundary layer

U   local velocity at edge of boundary layer

$\dfrac{u}{U}$ velocity ratio for incompressible flow $\left(\sqrt{\dfrac{H - p_{wall}}{H_{max} - p_{wall}}}\right)$

δ   boundary-layer thickness at 0.95u/U

δ*   boundary-layer displacement thickness for incompressible flow

$$\int_0^{\delta'} \left(1 - \frac{u}{U}\right)dy$$

θ   boundary-layer momentum thickness for incompressible flow

$$\int_0^{\delta'} \frac{u}{U}\left(1 - \frac{u}{U}\right)dy$$

δ'   distance from surface beyond which the contribution to the
                integral of δ* and θ is negligible

δ^*/θ boundary-layer-shape parameter for incompressible flow

Diffuser performance parameters:

$\Delta H/q_{c_1}$ loss coefficient

$\Delta q_c/\Delta q_{c_{ideal}}$ diffusion factor

$\Delta p/\Delta q_c$ pressure efficiency

$\Delta p/\Delta p_{ideal}$ diffuser effectiveness

Subscripts:

0   reference conditions

1   diffuser inlet conditions

6   diffuser (conical expansion) exit conditions

7   tail-pipe exit conditions

1 to 6   boundary-layer survey stations

APPARATUS AND TESTS

General arrangement.- The apparatus used for this investigation is shown in figure 1. It consists of a 23° conical diffuser joined to a cylindrical entrance duct 21 inches in diameter by a transition section having a radius of $5\frac{3}{16}$ inches and a tail pipe approximately $3\frac{1}{2}$ inlet diameters in length and having a diameter of 29.70 inches. Air was forced through the system by two centrifugal compressors. An arrangement, the same as that outlined in reference 5, was used in performing the tests.

The minimum length of the 21-inch entrance duct is approximately 0.4 inlet diameter. An additional section of about 4 inlet diameters was provided for insertion between the entrance bell and the smaller duct for the purpose of thickening the boundary layer. A photograph of the arrangement with the additional length of inlet duct is shown as figure 2.

The interior of the test apparatus was smoothly finished after being sprayed with several coats of paint. The dimensions of the junction between the inlet duct and the diffuser were arbitrarily chosen fairly short. The joint between the inlet section and diffuser was filled with pyroxylin and carefully finished to a $5\frac{3}{16}$-inch radius. The joint between the diffuser and tail pipe was finished in a similar manner to a $4\frac{11}{16}$-inch radius. During the course of this investigation neither of the filled joints was changed or altered.

A careful check of the dimensions of the diffuser upon completion of the tests showed that the maximum deviation from the prescribed dimensions were as follows:

(1) Inlet channel concentric within 0.010 inch at any position.

(2) Greatest error in conical portion of diffuser about 0.2° at any location.

(3) Exit cylindrical duct accurate within 1/16 inch at any position.

Instrumentation.— The positions at which all pressure surveys were made are shown in figure 1. Total—pressure—loss surveys were made at stations 1 and 7. Boundary—layer pressure surveys were made at stations 1 to 6, as indicated in figure 1. Flush—type static—pressure orifices were located in the inlet duct, diffuser, and tail pipe.

Detailed diagrams of the instruments used for the inlet—pressure— loss surveys and the boundary—layer pressure surveys are shown in figure 1. Difficulty was encountered in making total—pressure surveys at the diffuser exit, station 6, due to the unstable character of the flow around the periphery. However, it was found that the flow was stable at the tail— pipe exit, and pressure—loss surveys were made at that point. Three rakes with six tubes each were installed 120° apart in the same plane. Each rake extended about 6 inches into the stream. Reference total pressure was measured upstream of the inlet bell with a total—pressure tube.

The inlet pitot—static surveys and all boundary—layer surveys were made with the use of electrically driven, remotely controlled devices that could extend the pressure tubes into the stream in accurate increments of distance. Stagnation—temperature measurements were made by means of an iron—constantan thermocouple located upstream of the bell (fig. 1) and directly read on a sensitive potentiometer.

Testing procedure.— Each of the following series of pressure measure— ments was taken over the entire range of inlet Mach numbers in the following sequence:

(1) Measurements were made of the longitudinal—wall static—pressure and the tail—pipe—exit (station 7) total—pressure distribution from the fixed rakes.

(2) Boundary—layer total—pressure surveys were made by using the exploring tube at station 6 followed by similar procedure at stations 5, 4, 3, 2, and 1 in that order. (See fig. 1.)

(3) A pressure survey of station 1 (fig. 1) was made by using two exploring tubes spaced 120° apart on the circumference. Pitot—static tubes were used in order to obtain simultaneous indication of static and total pressure.

All pressure measurements were made with the use of multitube bank— type manometer boards.

METHODS AND ANALYSIS

Computational methods.— The requirement that the inlet duct and diffuser be free of all obstructions upstream of any station at which pressure measurements were in progress made it impossible to record simultaneous upstream and downstream measurements. The inlet-pressure ratio $\left(p_1/H_0\right)$ was used as a correlating parameter for the computation of the performance coefficients.

Performance parameters.— The mass-weighted mean loss in total pressure from the reference station 0 to the inlet station 1 was computed in this manner:

$$\overline{H_0 - H_1} = \Delta H_{0,1} = \frac{2\pi \int_0^r (\rho V)_y (H_0 - H_1)_y\, y\, dy}{2\pi \int_0^r (\rho V)_y\, y\, dy}$$

where the quantity $(\rho V)_y$ was computed by using the expression

$$(\rho V)_y = \sqrt{\left(\frac{2\rho}{F_c}\right)_y (H_1 - p_1)_y}$$

The quantity ρ/F_c can be obtained from p, T, H, and gas properties by the following relation:

$$\frac{\rho}{F_c} = \frac{\gamma}{\gamma - 1}\frac{H}{RT}\left[\frac{\left(\frac{p}{H}\right)^{\frac{2}{\gamma}} - \left(\frac{p}{H}\right)^{\frac{\gamma+1}{\gamma}}}{1 - \frac{p}{H}}\right]$$

The mean change in total pressure from the reference station 0 to the tail-pipe exit, station 7, was computed similarly, assuming the wall static pressure at the tail-pipe exit is constant in the transverse plane of that section. The mean total-pressure loss is obtained directly as the difference in total pressure between the tail-pipe exit and the diffuser inlet. Consequently, the mean loss in total pressure computed by this procedure includes both the losses in the conical expansion and the tail-pipe loss.

The rise in static pressure was computed as the difference between the arithmetic mean of the inlet static pressure obtained by stream surveys, and the wall static pressure at the measuring station (diffuser exit, station 6, and tail-pipe exit, station 7). The static pressure was assumed to be constant across the downstream measuring station.

The mean change in impact pressure between stations is determined as the rise in static pressure less the mean loss in total pressure. The theoretical gain in static pressure and change in impact pressure were computed by assuming frictionless one-dimensional flow.

RESULTS AND DISCUSSION

In subsequent discussion of the diffuser performance and boundary-layer characteristics, the terminology adopted as a means of identifying the two different inlet boundary-layer conditions is that of "thinner" and "thicker" inlet boundary layers. The thinner-inlet-boundary-layer case refers to the configuration which was tested with the cylindrical entrance duct of 8.25 inches in length, which had an inlet-boundary-layer thickness of about 1 percent of the inlet diameter. For the thicker-inlet-boundary-layer case, an inlet-boundary-layer thickness of about 5 percent of the inlet diameter was measured.

All performance curves are plotted against the inlet-pressure ratio p_1/H_0, a parameter chosen as an approximate index of the inlet Mach number. Increasing Mach number is denoted by rightward movement on the abscissa. No provision was made for the isolation of Mach number and Reynolds number effects. A curve of the inlet flow characteristics is presented in figure 3, which gives the variation of the weight flow and mean inlet Mach number with mean pressure ratio.

Diffuser performance parameters.— Since there are numerous applications for diffusers, the following coefficients are used in the analysis of results:

(1) The loss coefficient, defined as $\Delta H / q_{c_1}$, which is a measure of the total pressure that is lost in the diffuser in overcoming friction and turbulence

(2) The diffusion factor, defined as $\Delta q_{c_\text{actual}} \big/ \Delta q_{c_\text{ideal}}$, which is a measure of the amount of impact pressure available for conversion to static pressure, compared to that possible with frictionless flow

(3) The pressure efficiency, defined as $\Delta p_\text{actual} \big/ \Delta q_{c_\text{actual}}$, which is a measure of the amount of impact pressure actually converted to static pressure

(4) The diffuser effectiveness, defined as $\Delta p_\text{actual} \big/ \Delta p_\text{ideal}$, which is a measure of the over—all performance of the diffuser. This coefficient is a measure of the useful static pressure obtained at the diffuser outlet, expressed as a ratio to that theoretically possible. The diffuser effectiveness is the product of the diffusion factor and the pressure efficiency:

$$\frac{\Delta p_\text{actual}}{\Delta q_{c_\text{actual}}} \frac{\Delta q_{c_\text{actual}}}{\Delta q_{c_\text{ideal}}} = \frac{\Delta p_\text{actual}}{\Delta q_{c_\text{ideal}}} = \frac{\Delta p_\text{actual}}{\Delta p_\text{ideal}}$$

Pressure—Survey Results

As previously pointed out, difficulty in making pressure surveys at the end of the conical section, station 6, made it impossible to express accurately the diffuser efficiency at that point, in three of the four performance parameters, namely those embodying the term ΔH_actual. Since the loss in total pressure in the tail pipe alone could not be evaluated, only one performance parameter is presented for both the tailpipe exit, station 7, and the diffuser exit, station 6. It should be noted that computation of $\Delta p_\text{actual} \big/ \Delta q_{c_\text{actual}}$ and $\Delta q_{c_\text{actual}} \big/ \Delta q_{c_\text{ideal}}$

for further analysis may be accomplished for the diffuser exit, station 6, with the data presented by the following relations:

$$\left(\frac{\Delta p_{actual}}{\Delta q_{c_{actual}}}\right)_{1-6} = \cfrac{1}{1 - \cfrac{\left(\dfrac{\Delta H_{actual}}{q_{c_1}}\right)_{1-7}}{\left(\dfrac{\Delta p_{actual}}{\Delta p_{ideal}}\right)_{1-6}\left[1 - \left(\dfrac{A_1}{A_6}\right)^2\right]}}$$

and

$$\left(\frac{\Delta q_{c_{actual}}}{\Delta q_{c_{ideal}}}\right)_{1-6} = \frac{\left(\dfrac{\Delta p_{actual}}{\Delta p_{ideal}}\right)_{1-6}}{\left(\dfrac{\Delta p_{actual}}{\Delta q_{c_{actual}}}\right)_{1-6}}$$

It must be kept in mind that curves computed by this procedure include the loss in total pressure in both the diffuser and the tail pipe.

Loss coefficient $\Delta H / q_{c_1}$.— The variation of $\Delta H / q_{c_1}$ with inlet-pressure ratio for the two inlet-boundary-layer conditions is shown in figure 4. An increase in inlet velocity manifested an increase in $\Delta H / q_{c_1}$ for both inlet conditions. With the thinner inlet boundary layer, the values of $\Delta H / q_{c_1}$ increased in a continuous manner with increasing inlet Mach number from about 0.05 at an inlet Mach number of 0.17, to about 0.115 at an inlet Mach number of 0.70 (highest velocity investigated). For the case of the thicker inlet boundary layer, the values of $\Delta H / q_{c_1}$ are about twice those of the thinner inlet boundary layer at the lowest inlet Mach number and increase in a manner similar to that of the thinner inlet boundary layer with increasing inlet velocity. The data of reference 6 give a value of $\Delta H / q_{c_1}$ of about 0.135 for a diffuser with a total angle of expansion of 23° with a 2:1 area ratio.

In general, the values of $\Delta H/q_{c_1}$ obtained in the current experiment
are less than that predicted by reference 6, except for the case of the
thicker inlet boundary layer at the higher inlet Mach numbers. However,
no conclusions should be drawn from this comparision because of the wide
difference in the inlet-flow conditions between those of the reference
data and the current experiment. The values of $\Delta H/q_{c_1}$ have a tendency
toward constancy in the range of Reynolds number encountered in these
experiments unless they are accompanied by a change in flow pattern.
Therefore, the departure of the values of $\Delta H/q_{c_1}$ from a constant coef-
ficient is indicative of a progressively changing flow pattern, with
consequent increased total-pressure losses. Subsequent discussions of
the boundary-layer characteristics show that the character and extent of
the regions of separated flow must play an important part in determining
the losses in total pressure; however, the data at hand are not considered
sufficient to permit any conclusive statement as to the exact nature of
the mechanism involved.

Diffusion factor $\Delta q_c/\Delta q_{c_{ideal}}$.— The diffusion factor is shown in
figure 5 as a function of inlet-pressure ratio for both inlet-boundary-
layer conditions, measured at the tail-pipe exit, station 7. In the
case of the thinner inlet boundary layer, the values of $\Delta q_c/\Delta q_{c_{ideal}}$
are very close to unity at the low inlet Mach numbers and drop slightly
as the velocity is increased. This indicates that almost all the obtain-
able impact pressure is made available for conversion to static pressure
over the entire flow range. For the thicker-inlet-boundary-layer case,
the values of $\Delta q_c/\Delta q_{c_{ideal}}$ indicate that about 97 percent of the obtain-
able impact pressure is available for conversion to static pressure at
the tail-pipe exit, station 7, over the range of inlet Mach numbers.
Some of the remaining 3 percent of the obtainable impact pressure may
be recoverable in an additional length of tail pipe. This is because
the velocity profile at staion 7 exhibits more curvature and therefore
possesses more kinetic energy than would be the case with the 1/7 power
law for the velocity distribution, to which the flow will revert in a
sufficient length of straight pipe. This conclusion is supported by the
data presented by Peters (reference 2) which shows that the length of
tail pipe needed to reach the point of maximum pressure is more than
twice that used in the current experiment.

Pressure efficiency $\Delta p/\Delta q_c$.— The pressure efficiency is shown as
a function of inlet-pressure ratio for both inlet-boundary-layer con-
ditions, measured at the tail-pipe exit, station 7, in figure 6. The
values of $\Delta p/\Delta q_c$ for both inlet boundary-layer conditions decrease

with increasing inlet Mach number at approximately the same rate. The
curve for the thicker inlet boundary layer is approximately 90 percent
of that for the thinner inlet boundary layer. This effect may be attrib-
uted to the shape of the curves of $\Delta H/q_{c_1}$ (fig. 4) which also vary at

approximately the same rate for both inlet-boundary-layer conditions
when the inlet velocity was increased.

Diffuser effectiveness $\Delta p/\Delta p_{ideal}$.— The variation of the diffuser
effectiveness with inlet pressure ratio is shown in figure 7 for both
inlet-boundary-layer conditions, presented for both measuring stations.
With the thinner inlet boundary layer, the values of $\Delta p/\Delta p_{ideal}$
measured at the diffuser exit, station 6, were of the order of 0.90 at
an inlet Mach number of 0.17 and diminished smoothly to about 0.60 at
an inlet Mach number of 0.86 (highest velocity investigated). The values
of $\Delta p/\Delta p_{ideal}$ measured at the tail-pipe exit, station 7, are substan-
tially greater than that of the diffuser alone, being of the order of 0.95
at the lowest inlet Mach number and dropping to about 0.75 at the highest
velocity investigated. For the case of the thicker inlet boundary layer,
the values of $\Delta p/\Delta p_{ideal}$ measured at the diffuser exit, station 6, are
about 0.65 at the lowest inlet Mach number, tapering off to about 0.48
at the highest velocity. The values of $\Delta p/\Delta p_{ideal}$ measured at the
tail-pipe exit, station 7, dropped smoothly from about 0.85 to 0.75 when
the inlet Mach number was increased from minimum to maximum value. The
major influence on the rate of decrease of the values of $\Delta p/\Delta p_{ideal}$
measured at the tail-pipe exit, station 7, for the thinner inlet boundary
layer is the shape of the curve of $\Delta p/\Delta q_c$. Since the values of $\Delta q_c/\Delta q_{ideal}$
are practically unity for this condition, the curve of $\Delta p/\Delta p_{ideal}$ is
almost identical to the curve of $\Delta p/\Delta q_c$ (fig. 6). Therefore, the pressure
efficiency may be regarded as the diffuser effectiveness if the diffusion
factor is approximately unity. In the case of the thicker inlet boundary
layer, $\Delta p/\Delta p_{ideal}$, measured at the tail-pipe exit, station 7, is slightly
less than the values of $\Delta p/\Delta q_c$. The values of $\Delta p/\Delta p_{ideal}$ are influenced
by the slight departure from unity of the values of $\Delta q_c/\Delta q_{c_{ideal}}$ computed
for that condition.

Since the rate of decrease of the curves of $\Delta p/\Delta q_c$ is almost the
same for both inlet-boundary-layer conditions, its influence will be the
same for both cases.

It may be noted that the data for the curves of $\Delta p/\Delta p_{ideal}$ for
the thinner—inlet—boundary—layer case are extended to higher inlet Mach
numbers than those in the preceding figures. Furthermore, the data shown
in figure 7 represent the true conditions at each of the stations 6
and 7 because the values were directly computed from pressure measure-
ments made through static—pressure orifices located in the transverse
plane of each of these stations. Although no comprehensive determi-
nation of the extent to which the presence of the tail pipe might affect
the performance of the diffuser was made, it was found that for values
of p_1/H_0 in the neighborhood of 0.90, the difference in the values of
diffuser effectiveness, with and without the tail pipe, was negligible.

Longitudinal variation in static pressure.— The variation in static
pressure along the wall of the diffuser is shown in figure 8 for the
thinner inlet boundary layer and in figure 9 for the case of the thicker
inlet boundary layer. On both curves, this variation is shown for a
number of different inlet Mach numbers identified by the values of the
ratio of the inlet static pressure to reference total pressure.

These curves show a very pronounced drop in static pressure at the
junction of the inlet duct and diffuser, as would be expected from the
local wall curvature. The sharply favorable pressure gradient is immedi-
ately followed by a correspondingly strong adverse pressure gradient as
the flow enters the straight—walled section of the diffuser.

Although not too apparent in the scale of figure 8 or 9, the point
of minimum pressure is not found at the midpoint of the arc joining the
inlet duct and diffuser but is found to be displaced a short distance
downstream of the midpoint.

At the highest inlet velocity shown in figure 8, the pressure ratio
at the point of maximum velocity has a value indicative of supersonic
flow. The pressure ratio alone, however, cannot be taken as a precise
measure of the mean Mach number at that particular section. Since a
strong static—pressure gradient normal to the wall must exist in this
region, the decrease in static pressure outside the boundary layer is
necessarily less than that at the wall. Thickening of the inlet boundary
layer has the effect of diminishing the velocity increase which occurs
at points of convex curvature. This can be seen by comparing the curves
shown in figures 8 and 9 having an approximately common initial pressure
ratio.

Figure 10 shows more extensive longitudinal static—pressure
distribution. That part of figure 10 enclosed in the box applies to
the diffuser proper, for which more detailed data were given in the two
preceding figures. The curves in figure 10 have been derived from cross
plots of graphs like those presented in figures 8 and 9, in order to

permit superimposing static—pressure profiles for the thicker and
thinner inlet—boundary—layer conditions at common values of inlet—pressure
ratio. Longitudinal static—pressure profiles calculated for ideal one—
dimensional flows have been added for comparison purposes. From the
junction point of the inlet duct and diffuser in the downstream direction,
the static—pressure recovery for the thinner inlet boundary layer,
although still much less than that for the ideal, is somewhat greater
than observed for the case of the thicker inlet boundary layer.

The further gain in static pressure in the tail pipe is shown in
figure 10. At the highest inlet velocity, in the case of the thicker
inlet boundary layer, the rise in static pressure in the tail pipe is
fairly large in comparison to the total rise, being of the order of one—
third the total rise in static pressure. This appears to be the natural
consequence of a reattachment and flattening of the transverse velocity
profile as fully developed pipe flow is approached.

Boundary—Layer Results

Boundary—layer characteristics.— Previous discussion has associated
the performance of the diffuser with the development of the boundary
layer. The nature and behavior of the boundary layer at several stations
along the wall of the diffuser are presented for both initial boundary—
layer conditions.

As an aid in interpreting the boundary—layer results obtained in
this investigation, the current physical picture of turbulent separation
is briefly reviewed. When a stream proceeds into a region of increasing
static pressure, the force due to the pressure gradient opposes the
flow. Excess of this opposing force over the shear forces associated
with transverse gradients of longitudinal velocity is balanced by reduc—
tion in momentum of the fluid. Equilibrium of forces is achieved,
therefore, by a retardation of the flow. If the momentum of the fluid
relative to zero velocity is insufficient to establish equilibrium, the
flow must reverse in direction. Under ordinary circumstances such
reversals in streams flowing against an adverse pressure gradient arise
in the boundary layer where the momentum is less than that of the main
stream. Under these conditions, the main stream, which does not experi—
ence a reversal in direction of flow, is said to have "separated" from
the wall of the channel. Separated flow is usually quite unstable, and
the conditions described are seldom if ever either steady or uniformly
distributed about the perimeter of even the most nearly symmetrical
channel.

Boundary—layer velocity profiles, under the action of an adverse
pressure gradient, are distorted by the local retardations and flow
reversals which occur. Typical profiles are shown in figure 11. Pro—
file (a) is representative of a boundary—layer flow at constant pressure.
Profile (b) is an example of clearly separated flow obtained in a region

of adverse pressure gradient. Profiles (c) and (d) are typical of those encountered in regions of adverse pressure gradient in which actual reversal has not yet occurred, at least on the point on the circumference at which the profile was measured. The appearance of either profile (c) or (d) is frequently regarded as evidence that separation is imminent or has occurred elsewhere on the circumference. As is shown subsequently, profile (d), which is of particular interest because of the appearance of a high velocity very close to the wall, may be obtained simultaneously with profile (c) at the same longitudinal position in a symmetrical diffuser but at a point somewhat removed circumferentially. Precise determination of the point of initial separation of flow in an adverse pressure gradient presents much difficulty because of the appearance of asymmetry in the flow pattern. Although observation of a profile such as (b) clearly establishes separation, failure to observe such a profile cannot be taken unreservedly as proof of the absence of separation but merely indicates that measurements were not made at the point on the circumference at which separation is occurring.

Since the shape of the velocity profile is indicative of the condition of the boundary layer, the value of form parameter derived from the profile bears a definite relationship to the approach of the separation point. It is shown by Von Doenhoff and Tetervin (reference 7) from two-dimensional data that the shape of all turbulent-boundary-layer profiles can be expressed, with fair accuracy, as a function of a single parameter. This shape parameter has been found to be the ratio of the boundary-layer displacement thickness to the momentum thickness. It is stated in reference 7 that separation was never observed at a value of this ratio less than 1.80 and appears definitely to have occurred for shape-parameter values greater than 2.60. It is further explained that it is impossible to fix these values accurately because the turbulent separation point is not clearly defined.

Methods of presentation.— In subsequent discussion of the boundary-layer results presented in figures 12 to 22, the results of the thicker-inlet-boundary-layer investigation are discussed before those of the thinner-inlet-boundary-layer configuration.

The velocity profiles computed from the pressure measurements made at six points along the wall of the duct (fig. 1) are presented in figures 12 and 14 for thicker and thinner inlet boundary layers, respectively. For most of the profiles shown in figures 12 and 14, computation of the boundary-layer thickness, displacement thickness, momentum thickness, and shape parameter has been made. For these computations no corrections for compressibility are introduced in order to present results comparable with the bulk of existing data. Since the calculation of boundary-layer parameters is meaningless for separated profiles, these have been omitted. The separated profiles are presented

for illustrative purposes only. As an aid in discussing the profiles
shown in figures 12 and 14, the computed boundary-layer parameters are
graphically represented as a function of inlet-pressure ratio in fig-
ures 18, 19, and 20. The variation of displacement thickness δ^*,
momentum thickness θ, and shape parameter δ^*/θ with pressure ratio
is shown in figure 18 for the thicker-inlet-boundary-layer case, and
figures 19 and 20 for the thinner-inlet-boundary-layer configuration.

Thicker inlet boundary layer.- Figures 12(a) to 12(f) represent
typical velocity profiles occurring at each of the six stations in the
diffuser for five inlet velocities. At station 1 (fig. 12(a)) the
boundary-layer thickness δ diminishes slightly with increasing velocity.
This apparent thinning of the boundary layer is reflected in the values
of the displacement thickness δ^* which are reduced about 25 percent
from the minimum to maximum inlet Mach number. The velocity profiles
at station 2 are shown in figure 12(b). A comparison of the values of
the displacement thickness δ^* of stations 1 and 2 (figs. 12(a), 12(b),
and 18) shows that the boundary layer has thickened about 40 percent at
the lower inlet Mach numbers, with the percentage of thickening becoming
more pronounced at the higher inlet velocities. Examination of the
values of the displacement thickness δ^* given in figure 18 shows that
in the presence of a slightly positive pressure gradient (station 1) the
values of the displacement thickness δ^* decrease with velocity. At
station 2, under the action of an unfavorable pressure gradient the
displacement thickness δ^* increases somewhat with inlet velocity.
Although no evidence of flow separation is indicated by the shape of the
velocity profiles at station 2, tuft surveys showed that the origin of
detached flow is slightly upstream of this point of circumferential
locations other than that at which the boundary-layer pressure surveys
were made over the entire speed range. The velocity profiles at
station 3 (fig. 12(c)) show appreciable thickening of the boundary layer,
and all are indicative of incipient separation. However, no evidence
of reverse flow is found at this point. As shown in figure 12(d), the
profiles at station 4 are, in almost all cases, separated from the wall
of the diffuser. The disturbed nature of the flow at this point is such
that the measurements in the vicinity of zero velocity lose significance.
This may distort the true values at points somewhat removed from the
wall, although the fluctuations are a much smaller proportion of the
mean flow. Examination of the profile shapes at stations 4 to 6
(figs. 12(d) to 12(f)) shows that flow separation has occurred at these
stations at all inlet Mach numbers. As pointed out previously, the
appearance of separation at one point on the wall in a single cross
section does not necessarily indicate the existence of separation at
other circumferential locations. Pressure surveys were made at several
points on the circumference in the transverse plane of station 6 to
verify the existence of asymmetrical boundary-layer flow conditions.
Velocity profiles computed from pressure surveys made at 120° intervals

on the periphery at station 6 are shown in figure 13. The profiles
corresponding to those presented in figure 12(f) were made at position (c).
The flow pattern varies with air flow, as evidenced by the similar,
although less pronounced, characteristics exhibited by the profile at
position (a) for the higher inlet velocity.

Thinner inlet boundary layer.— A set of figures similar to those
presented for the thicker inlet boundary layer are given for the thinner
inlet boundary layer (figs. 14(a) to 14(f)). In general, the flow con-
ditions which were pointed out in detail in the case of the thicker inlet
boundary layer are shown to exist to a lesser degree in the thinner-
inlet—boundary—layer configuration. There are, however, certain figures
which show unusual characteristics not covered in the case of the thicker
inlet boundary layer.   •

From the profiles at station 1 (fig. 14(a)) it can be seen that the
profiles are considerably thinner at all inlet Mach numbers than those
shown for the thicker inlet boundary layer at station 1 (fig. 12(a)),
the displacement—thickness values actually being about one—fifth those
computed for the thicker inlet boundary layer. The displacement—
thickness values for both inlet—boundary—layer cases show a similar
reduction of about 25 percent as the velocity is increased from minimum
to maximum value (figs. 18 and 19). As in the case of the thicker inlet
boundary layer at station 2, an upward trend of the displacement—thickness
values is indicated with increasing inlet Mach number (fig. 19). Retar-
dation of the flow near the wall is first discernible at station 3
(fig. 14(c)). At the three highest inlet velocities shown at station 5,
(fig. 14(e)) velocities as high as 50 percent of local stream velocity
are shown at the measurement point closest to the wall. Separated
boundary layers are shown at all inlet Mach numbers at station 6
(fig. 14(f)). A sudden reduction in the thickness of the boundary
layer at the highest velocity (fig. 14(f)) may be indicative of the
reestablishment of attached flow at this point on the circumference,
with possible separation at other circumferential locations. Velocity
profiles at three points on the periphery at the exit, station 6, are
shown in figure 15 for two inlet Mach numbers. As shown in the case of
the thicker inlet boundary layer, flow asymmetry exists at this point.
Boundary—layer separation is apparent at position (c) for both air flows,
as was the case with the thicker inlet boundary layer for both inlet
Mach numbers. The asymmetrical flow conditions are associated with a
shifting flow pattern throughout the diffuser. Upon repetition of some
of the boundary—layer measurements at certain locations, different
profiles were found in some cases at the same airspeed and station.
The occurrence of both separated and unseparated velocity profiles at
station 2, at approximately the same inlet velocity, is shown in figure 16.
The radically different profiles observed at station 5 at almost constant
inlet Mach number are shown in figure 17. From the results presented in
figures 15, 16, and 17, it may be surmised that the separated zone may not
only vary with airspeed but also with time.

By using the faired values of boundary—layer thickness derived from
the profiles in figures 12 and 14, the longitudinal variation in boundary—
layer thickness δ is shown in figure 21. Curves are given for both
inlet—boundary—layer thicknesses at three inlet Mach numbers. In the
case of the thicker inlet boundary layer the curves for all air flows
appear smooth. The thickness increases substantially as the distance
from the inlet is increased. In the case of the thinner inlet boundary
layer, excessive thickening of the boundary layer as a result of sepa—
rated flow at the exit causes a rather steep increase in the curves at
that point. At the highest velocity shown (fig. 21(c)) the unusual shape
of the boundary—layer—thickness curve for the thinner inlet boundary
layer is suggestive of the growth of a separate disturbance in the exit
regions of the diffuser. The data obtained in the present paper are not
complete enough to furnish even a qualitative analysis of the nature of
the secondary flow in a separated region. Referring to figure 21(c),
the slightly larger exit boundary layer for the thinner—inlet—boundary—
layer case is a consequence of the asymmetrical flow conditions which
exist in this region. From the velocity profiles shown in figures 13
and 15, a comparison of the distribution of the boundary—layer thick—
ness δ at station 6 for both configurations is presented in figure 22.
It can be seen from these curves that at both inlet Mach numbers shown,
a greater area is bounded by the curve representing the thinner inlet
boundary layer. This is in accord with the performance results previously
discussed. Although the core enclosed by the curves of the boundary—
layer thickness may not be taken as an actual measure of the effective
area of the air stream, they are indicative of the relative position of
the nucleus of the high—energy air. Both inlet—boundary—layer conditions
exhibited a tendency toward concentration of the flow on the left side
of the duct, the observer looking in an upstream direction. This may
be attributed to slight geometric imperfections in the test apparatus.

A correlation of all the values of shape parameter obtained in this
investigation is as follows. The range of shape—parameter values obtained
for each type of profile shown in figures 11(a) to 11(d) is indicated.
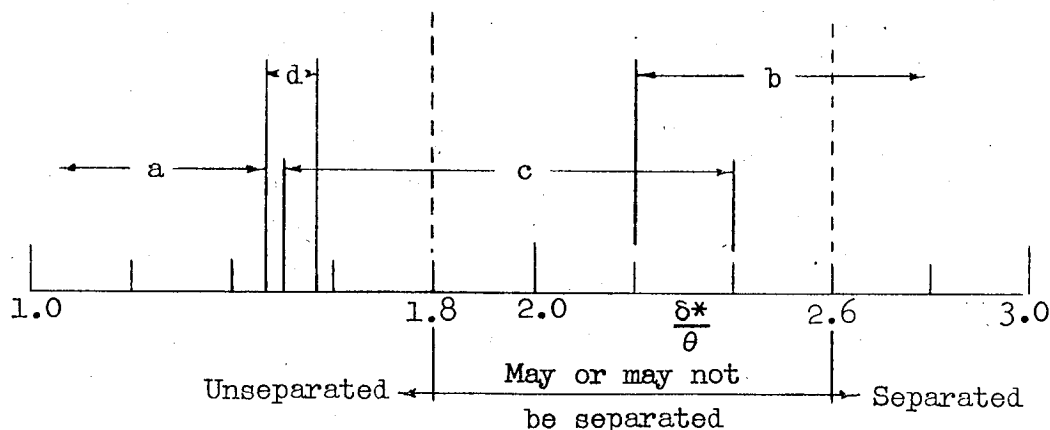
In comparing the values of shape parameter for different types of profiles with the limits set forth in reference 7, fair agreement is found, although the complete band of values corresponding to different types of profiles obtained in the current experiment is displaced several points toward the unseparated region of the range indicated by reference data.

CONCLUSIONS

From the current investigation regarding the effect of the inlet Mach number and initial boundary-layer thickness on the performance and boundary-layer characteristics of a 23° 21-inch conical diffuser – tail-pipe combination with a 2:1 area ratio, the following conclusions are drawn:

1. With the thinner inlet boundary layer (mean value of inlet displacement thickness about 0.034 in. over the speed range), the total-pressure losses increased in a continuous manner with increasing inlet Mach number from about 5 percent of inlet impact pressure at an inlet Mach number of 0.17, to $11\frac{1}{2}$ percent at an inlet Mach number of about 0.70 (highest velocity investigated).

2. With the thicker inlet boundary layer (mean value of inlet displacement thickness about 0.170 in. over the speed range), the total-pressure losses expressed as a fraction of inlet impact pressure are approximately twice those of the thinner inlet boundary layer at the lowest inlet Mach number. Increasing the inlet Mach number increased the total-pressure losses in a manner similar to that of the thinner inlet boundary layer.

3. With the thinner inlet boundary layer, the static-pressure rise measured at the diffuser exit is of the order of 90 percent of the ideal value at an inlet Mach number of 0.17 and diminishes smoothly to about 60 percent of the ideal value at an inlet Mach number of 0.86 (highest velocity investigated).

4. For the case of the thicker inlet boundary layer, the static-pressure recovery at the diffuser exit is about 65 percent of the ideal value at the lowest inlet Mach number, dropping smoothly to about 48 percent of the ideal value at the highest velocity investigated.

5. With the thinner inlet boundary layer, the rise in static pressure in the tail pipe is of the order of 5 percent of the over-all rise at the lower inlet Mach numbers, increasing to approximately 20 percent of

the over-all rise at the highest velocity investigated. With the
thicker inlet boundary layer, the tail pipe contributed an average
static-pressure rise of about 25 percent of the over-all rise throughout
the entire flow range.

6. At the tail-pipe exit, the impact-pressure conversion is within
a few percent of that ideally possible for both inlet boundary-layer
thicknesses over the entire flow range.

7. Flow separation was observed within the diffuser for both inlet-
boundary-layer thicknesses at all inlet Mach numbers.

In the case of the thinner inlet boundary layer, flow separation
occurred at the diffuser exit over the entire speed range. At the
higher inlet Mach numbers, unseparated flow alternating with separated
flow was observed as far upstream as station 2.

With the thicker inlet boundary layer, indications of separated
flows were found slightly downstream of the inlet-duct-diffuser junction
at all inlet velocities.

8. The values of boundary-layer shape parameter show fairly good
agreement with those obtained from airfoil data taken at velocities
comparable to those encountered in the current investigation.

Langley Aeronautical Laboratory
        National Advisory Committee for Aeronautics
                Langley Air Force Base, Va.

REFERENCES

1. Gibson, A. H.: On the Flow of Water through Pipes and Passages
     Having Converging or Diverging Boundaries. Proc. Roy. Soc.
     (London), ser. A, vol. 83, no. 563, March 2, 1910, pp. 366–378.

2. Peters, H.: Conversion of Energy in Cross–Sectional Divergences
     under Different Conditions of Inflow. NACA TM 737, 1934.

3. Kröner, Richard: Versuche über Strömungen in stark erweiterten
     Kanälen. Forsch.–Arb. Geb. Ing.–Wes. VDI–Verlag G.m.b.H. (Berlin),
     Heft 222, 1920, pp. 1–85.

4. Vedernikoff, A. N.: An Experimental Investigation of the Flow of
     Air in a Flat Broadening Channel. NACA TM 1059, 1944.

5. Copp, Martin R., and Klevatt, Paul L.: Investigation of High–Subsonic
     Performance Characteristics of a 12° 21–Inch Conical Diffuser,
     Including the Effects of Change in Inlet–Boundary–Layer Thickness.
     NACA RM L9H10, 1950.

6. Henry, John R.: Design of Power–Plant Installations. Pressure–Loss
     Characteristics of Duct Components. NACA ARR L4F26, 1944.

7. Von Doenhoff, Albert E., and Tetervin, Neal: Determination of
     General Relations for the Behavior of Turbulent Boundary Layers.
     NACA Rep. 772, 1943.
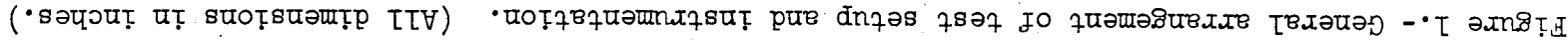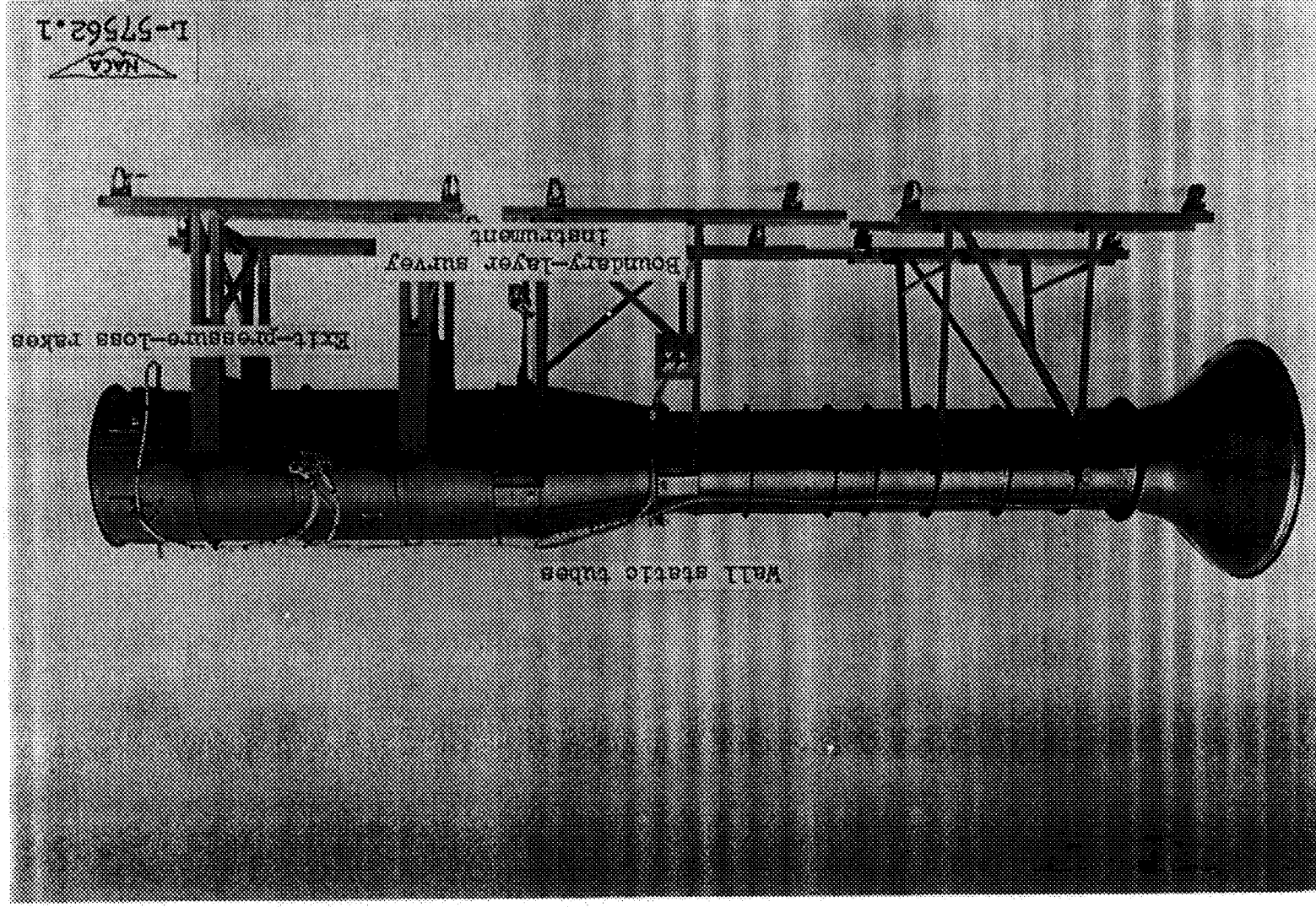
Figure 2.- Photograph of diffuser with long inlet.
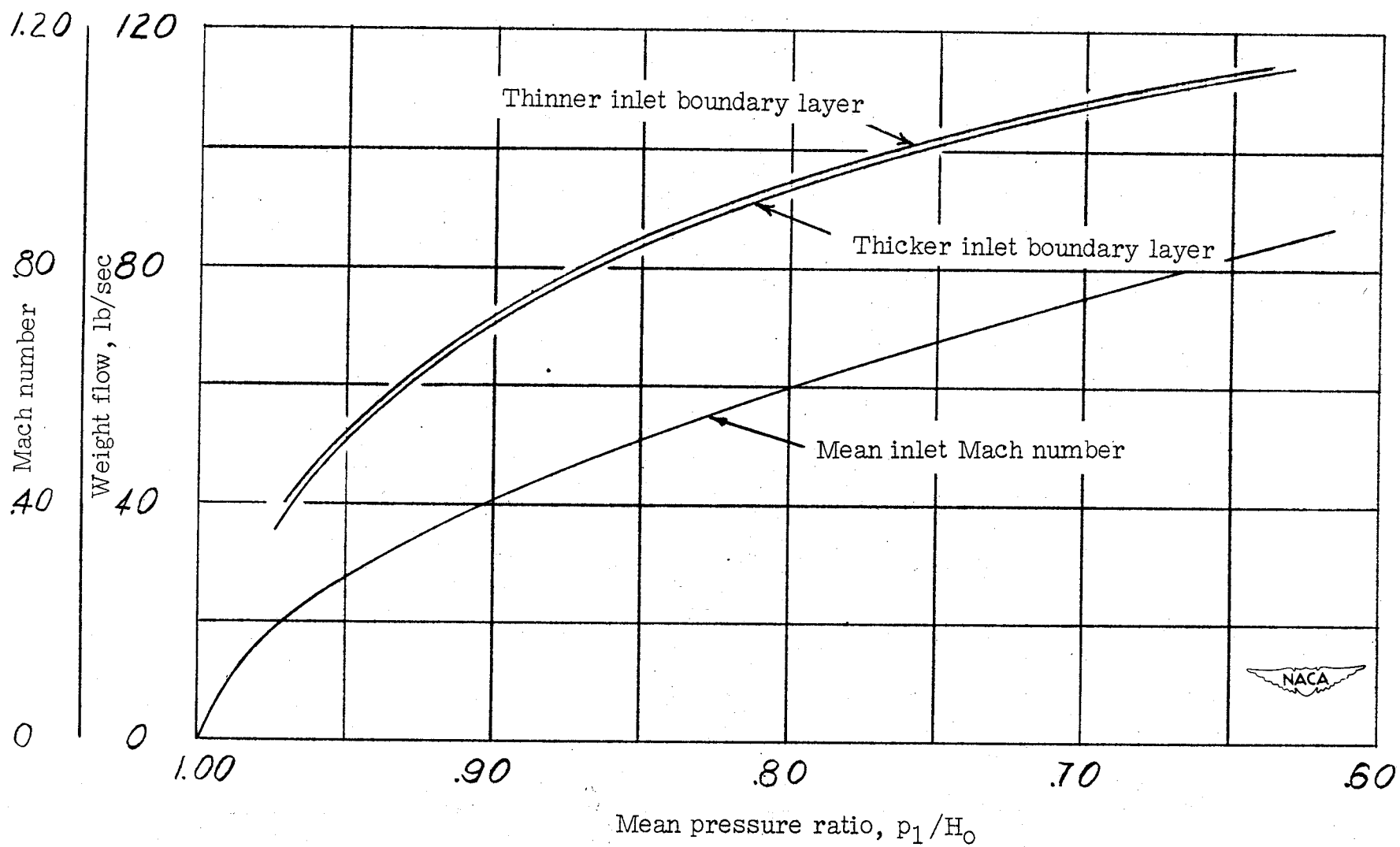
Figure 3.- Inlet-flow characteristics.
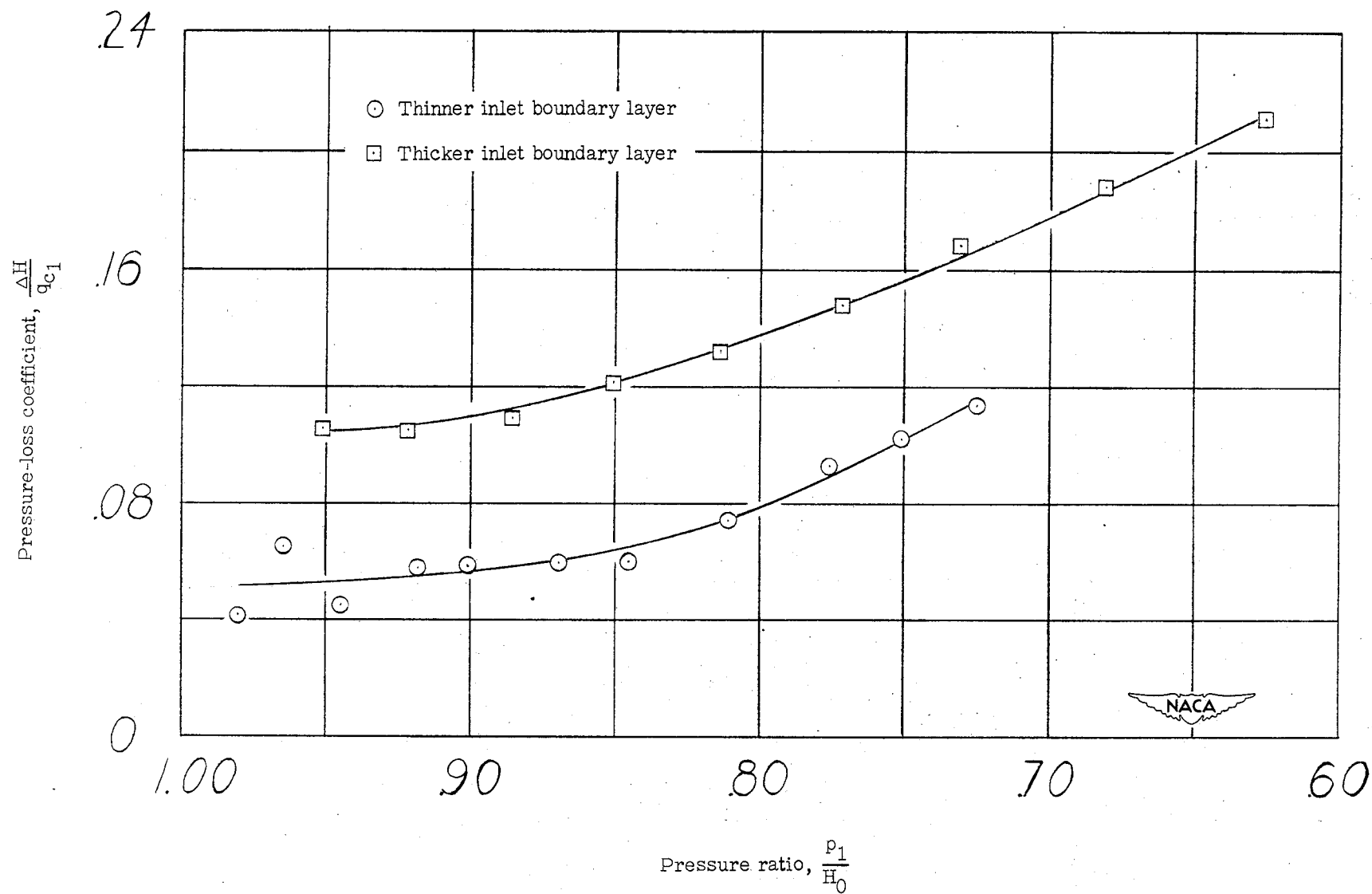
Figure 4.- Variation of pressure-loss coefficient with pressure ratio.
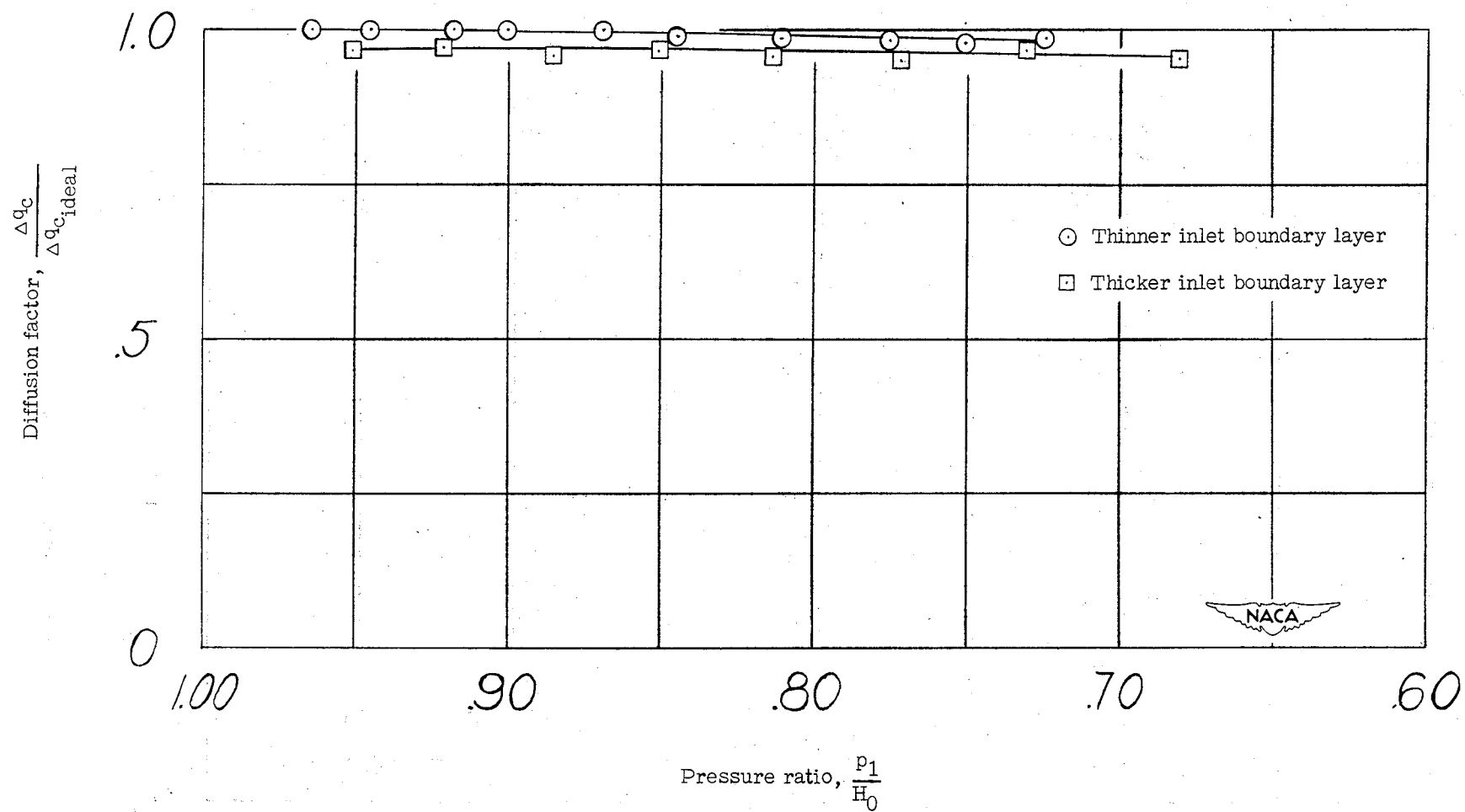
Figure 5.- Variation of diffusion factor with pressure ratio.
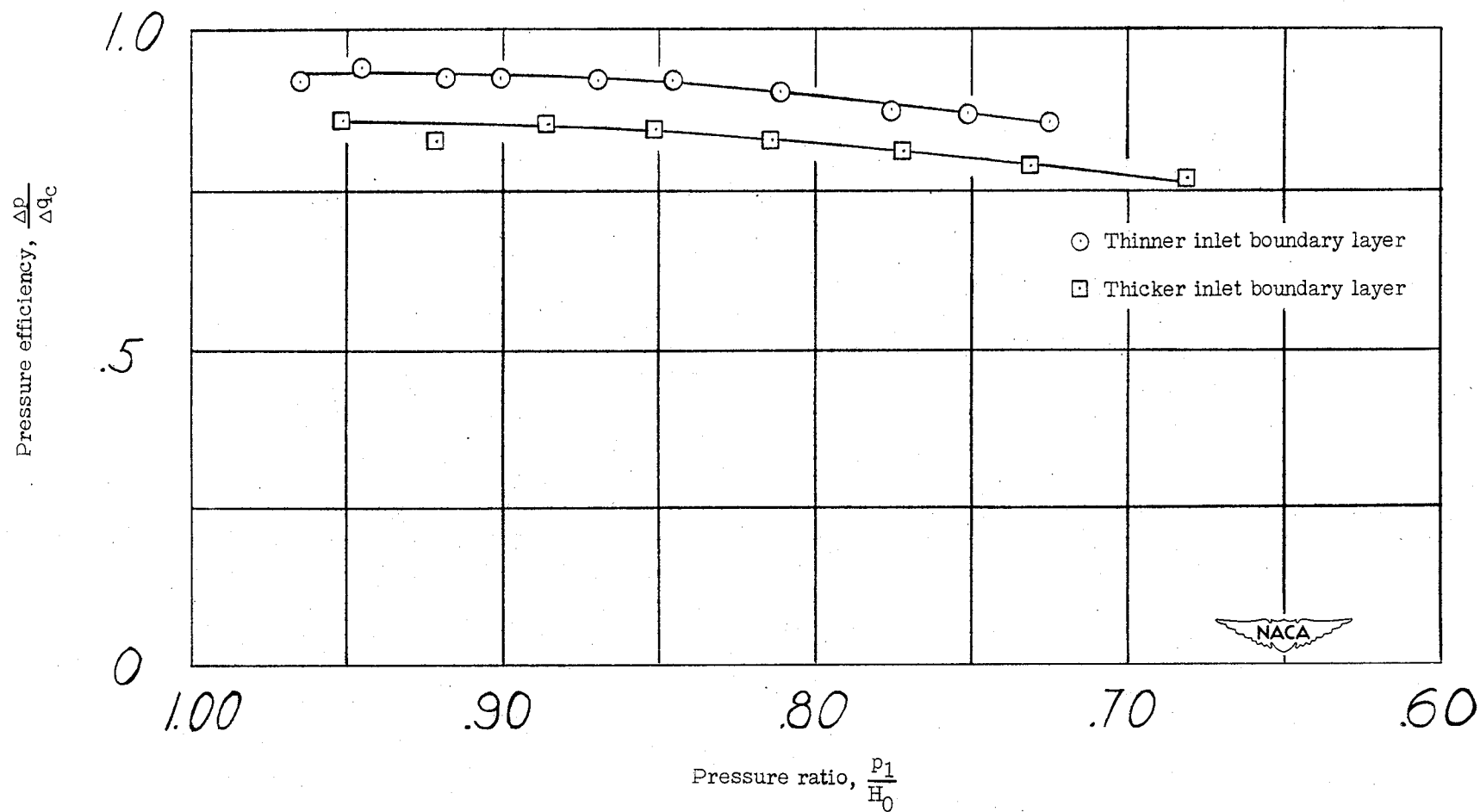
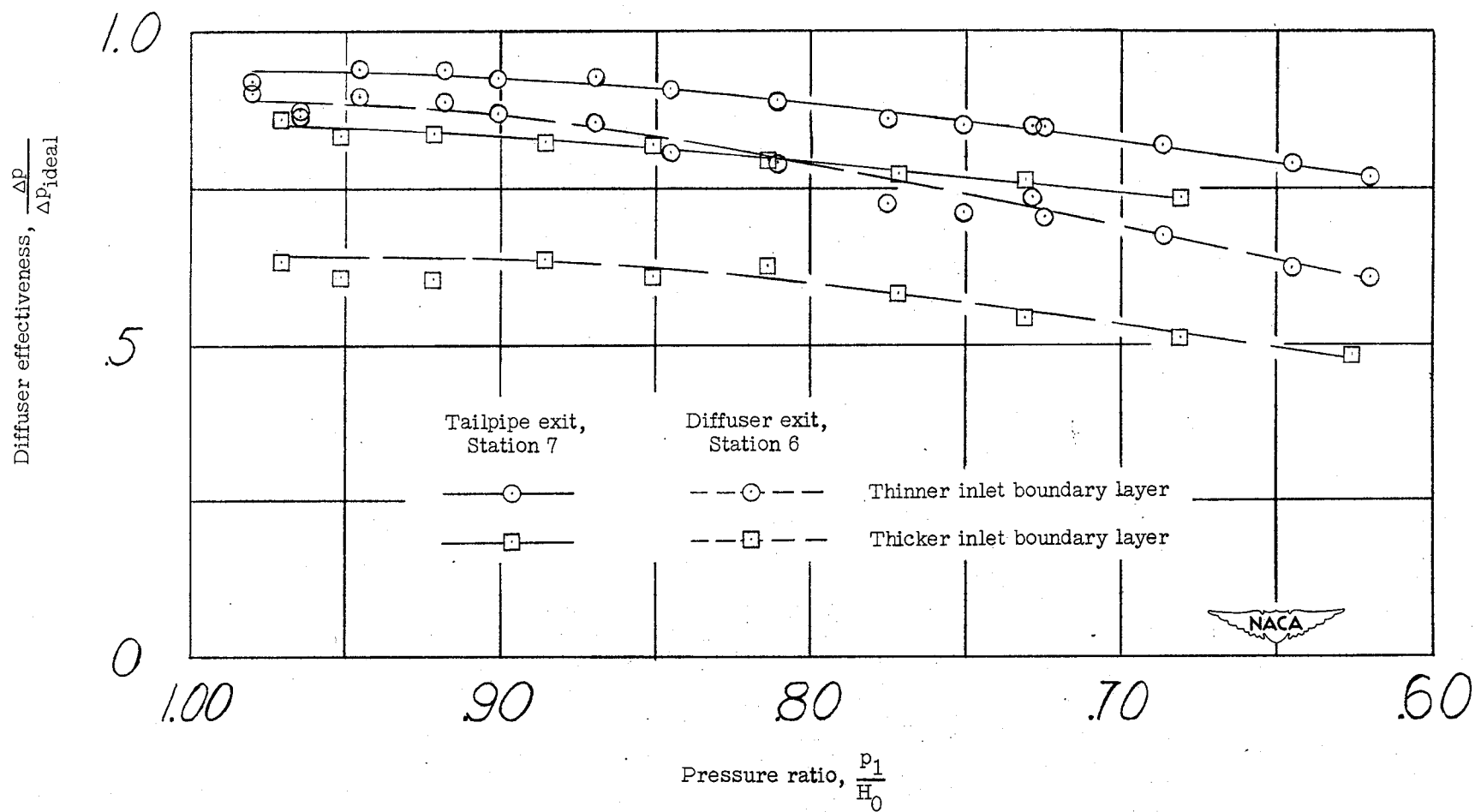Figure 6.- Variation of pressure efficiency with pressure ratio.

Diffuser effectiveness, $\dfrac{\Delta p}{\Delta p_{ideal}}$

Tailpipe exit,
Station 7

Diffuser exit,
Station 6

Thinner inlet boundary layer

Thicker inlet boundary layer

NACA

Pressure ratio, $\dfrac{p_1}{H_0}$

Figure 7.- Variation of diffuser effectiveness with pressure ratio.
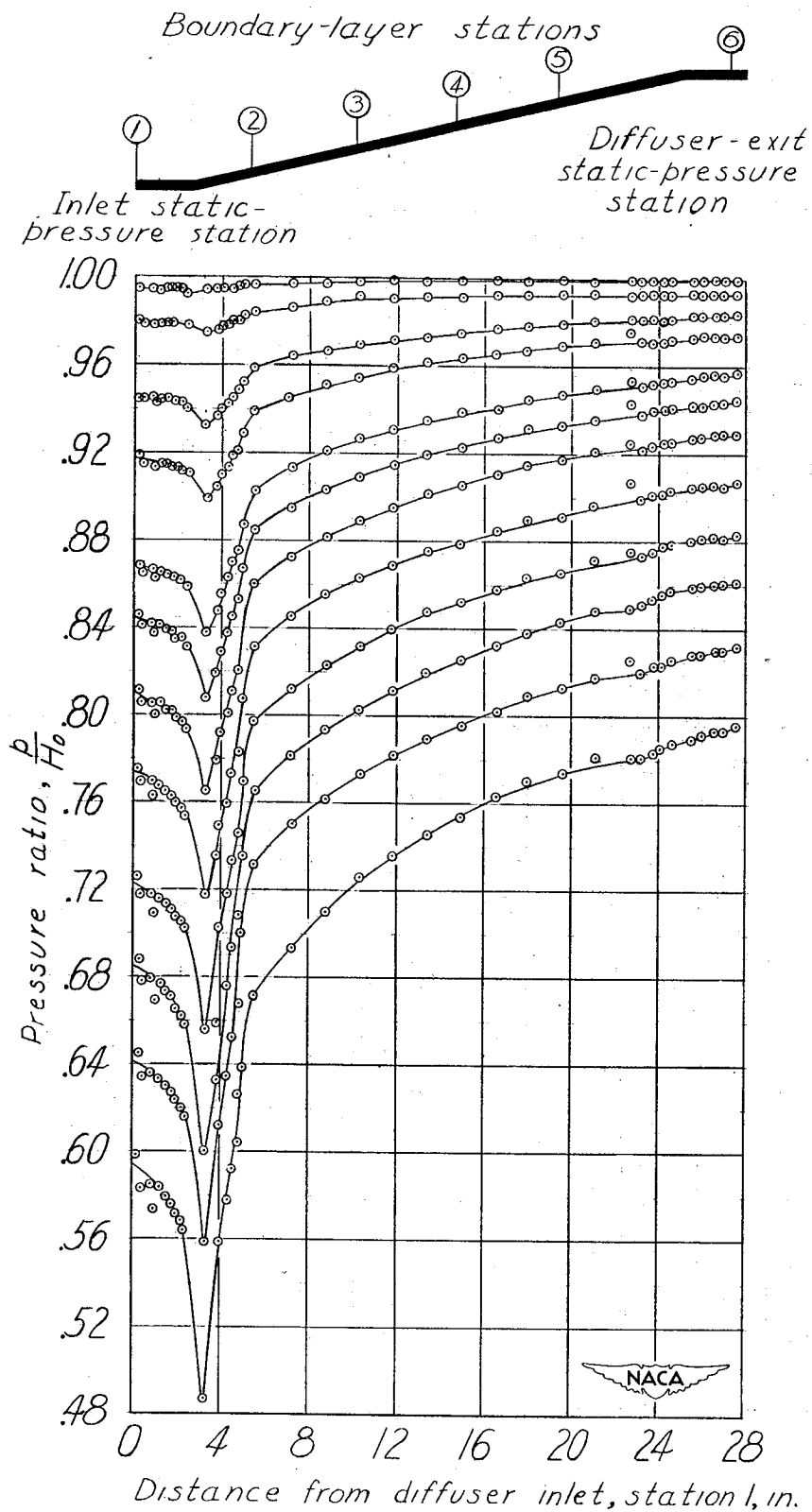
Figure 8.- Static-pressure distribution of diffuser. Thinner inlet
boundary layer.
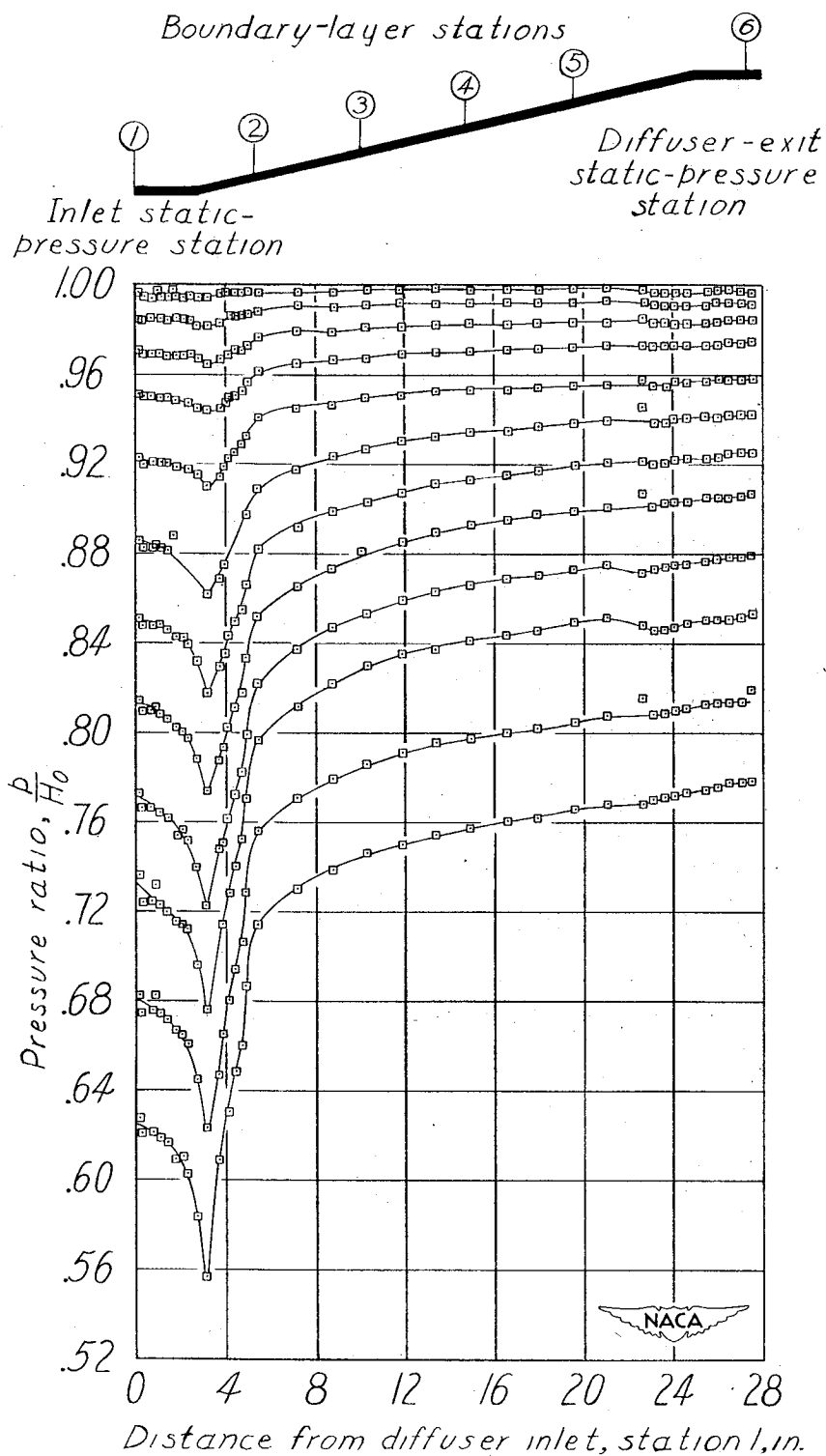
Figure 9.- Static-pressure distribution of diffuser. Thicker inlet
boundary layer.

Boundary-layer stations

① ② ③ ④ ⑤ ⑥ ⑦

Inlet static-
pressure station

Diffuser-exit
static-pressure
station

Tail-pipe-exit
static-pressure
station

Thinner inlet boundary-layer

Thicker inlet boundary-layer

Ideal one-dimensional distribution

Distance from diffuser inlet, station 1, in.
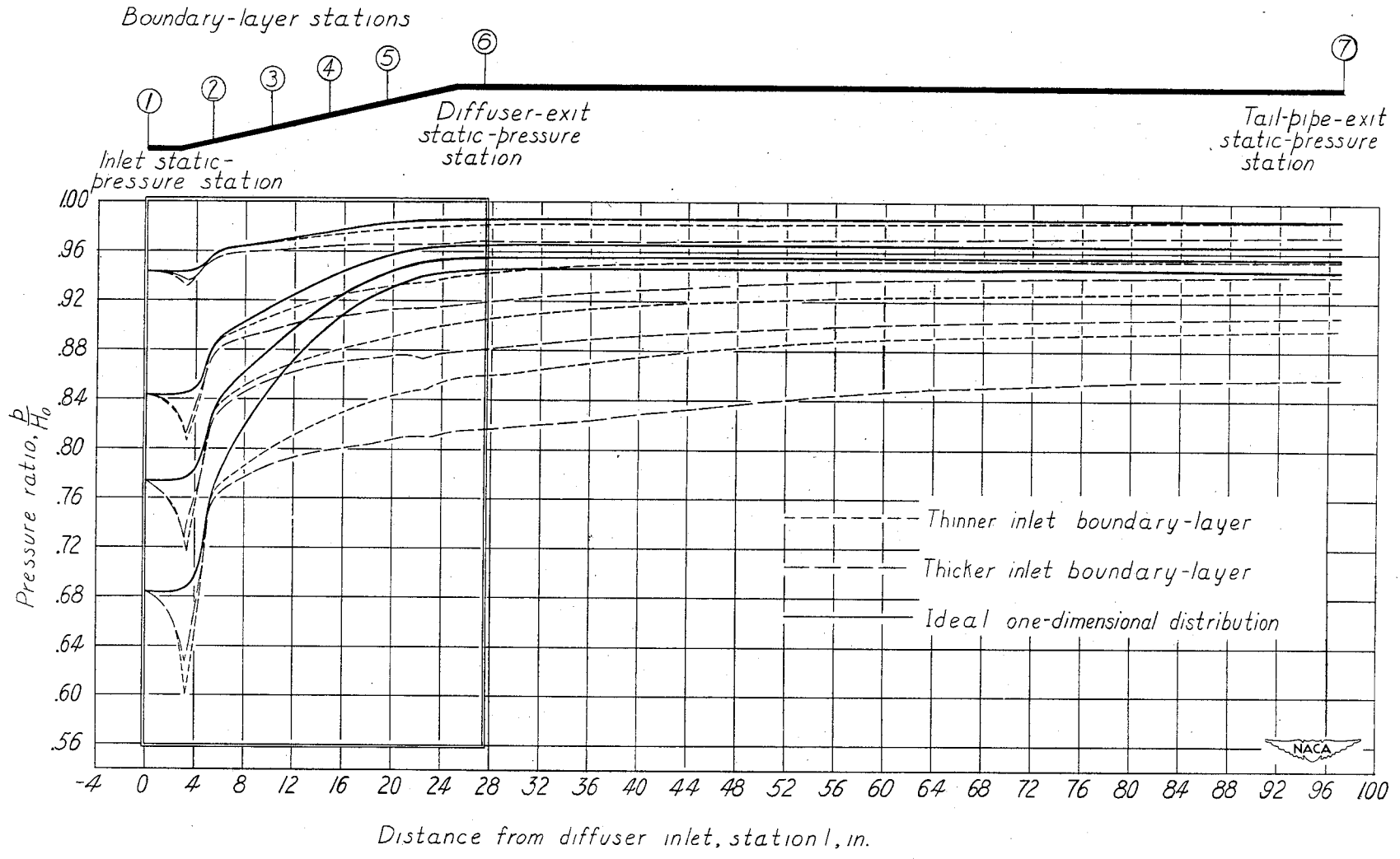
Figure 10.- Static-pressure distribution of diffuser and tail pipe. Both inlet boundary-
layer thicknesses.
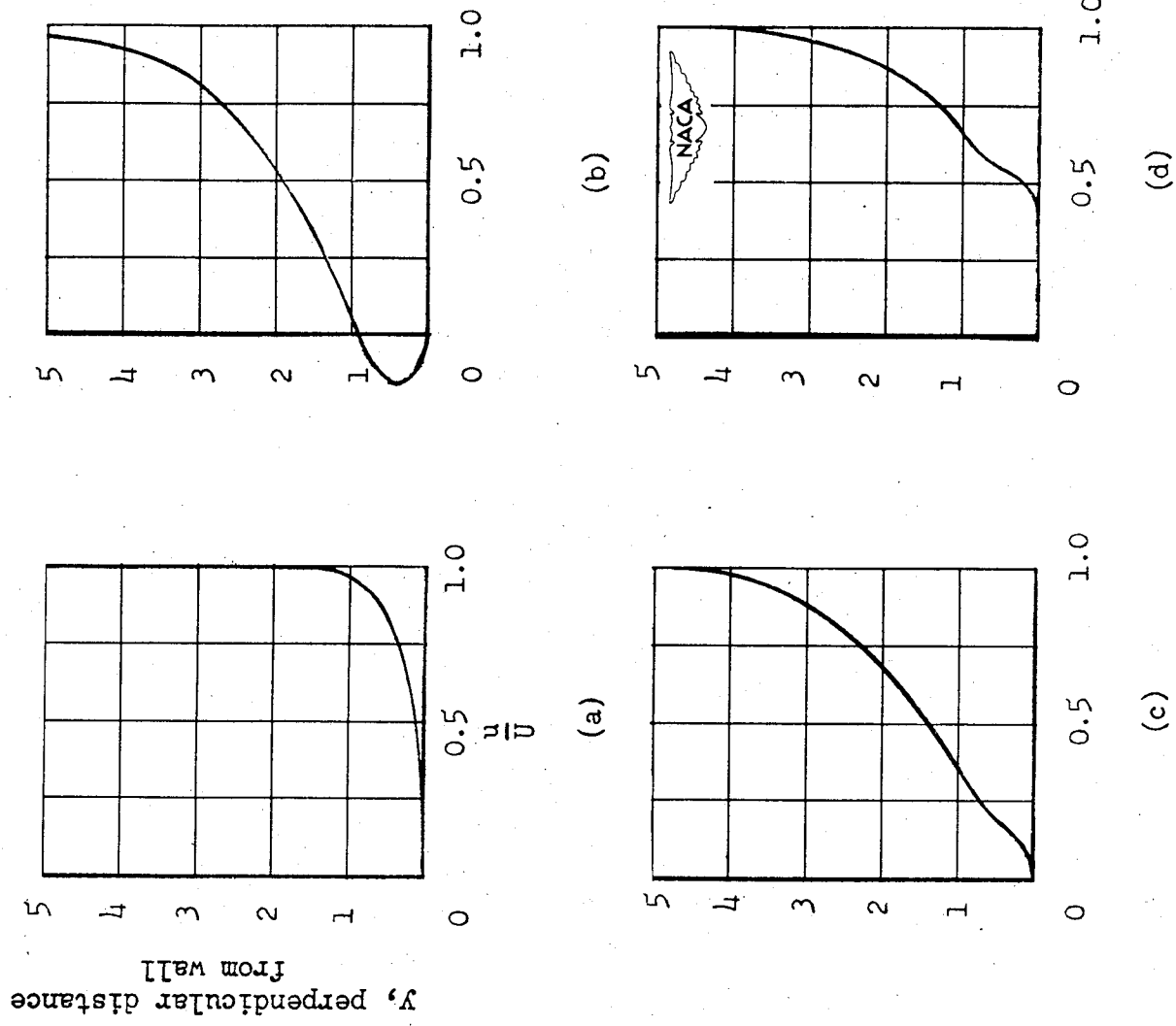
Figure 11.- Typical turbulent-boundary-layer velocity profiles.

y, perpendicular distance from diffuser wall, in.

$$\frac{p_1}{H_0} = 0.9510$$

$\delta = 1.06$
$\delta^* = 0.200$
$\theta = 0.164$
$\dfrac{\delta^*}{\theta} = 1.22$

$$\frac{p_1}{H_0} = 0.8330$$

$\delta = 1.01$
$\delta^* = 0.198$
$\theta = 0.158$
$\dfrac{\delta^*}{\theta} = 1.25$

$$\frac{p_1}{H_0} = 0.7770$$

$\delta = 0.92$
$\delta^* = 0.156$
$\theta = 0.122$
$\dfrac{\delta^*}{\theta} = 1.28$

$$\frac{p_1}{H_0} = 0.7200$$

$\delta = 0.86$
$\delta^* = 0.149$
$\theta = 0.116$
$\dfrac{\delta^*}{\theta} = 1.29$

$$\frac{p_1}{H_0} = 0.6316$$

$\delta = 0.85$
$\delta^* = 0.151$
$\theta = 0.118$
$\dfrac{\delta^*}{\theta} = 1.28$

$\dfrac{u}{U}$

NACA
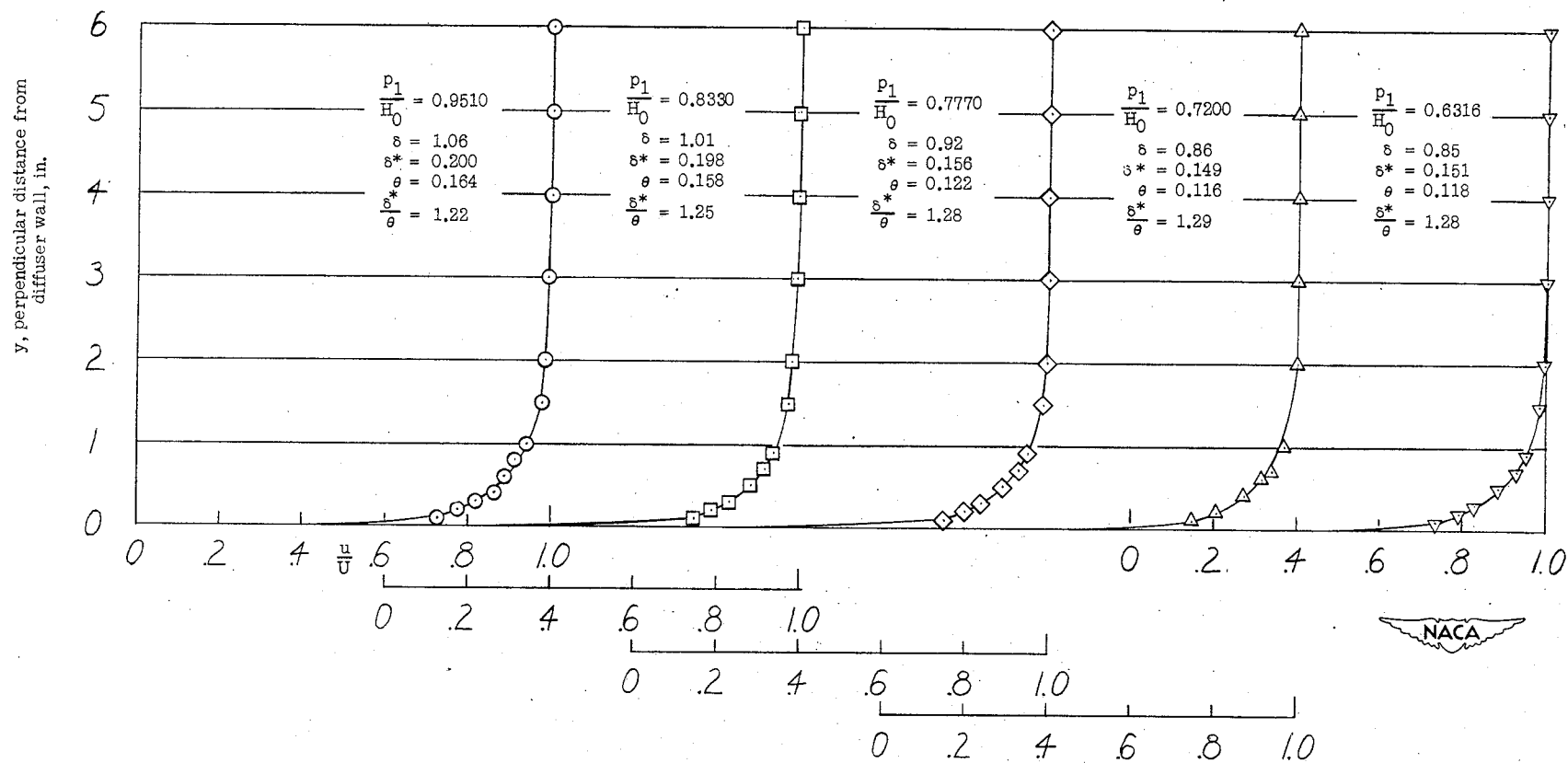
(a) Station 1.

Figure 12.- Boundary-layer velocity profiles. Thicker inlet boundary layer.
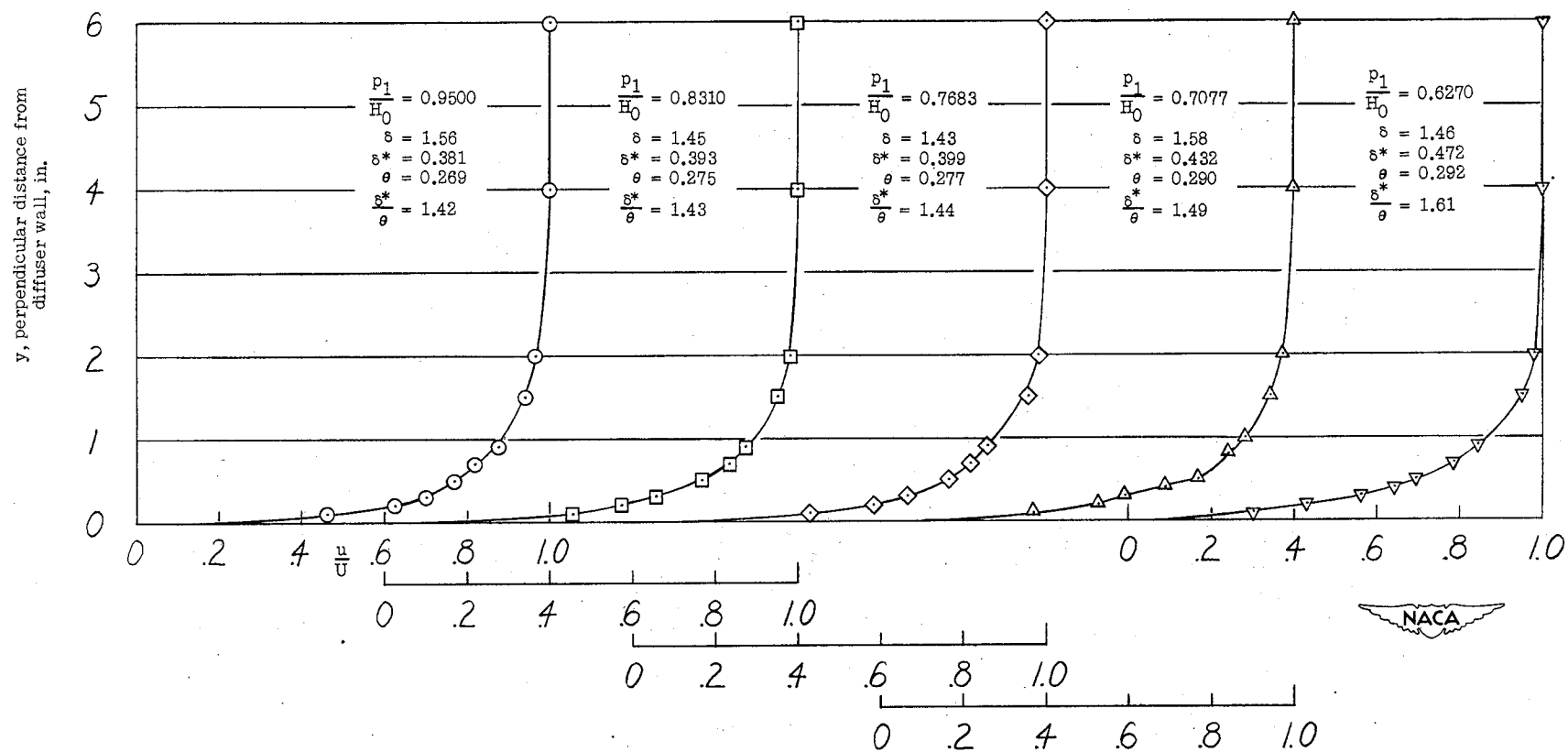
(b) Station 2.

Figure 12.- Continued.
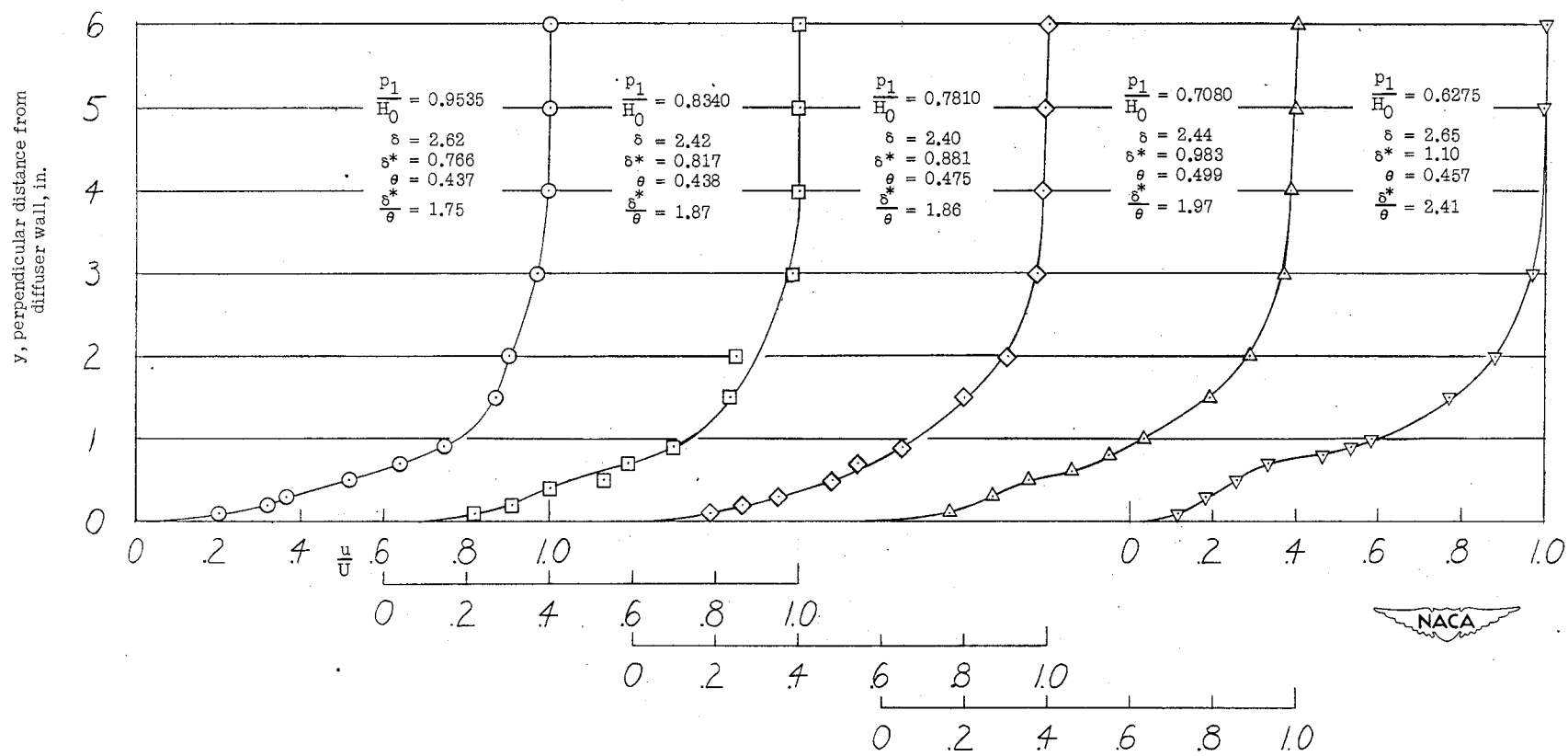
(c) Station 3.

Figure 12.- Continued.
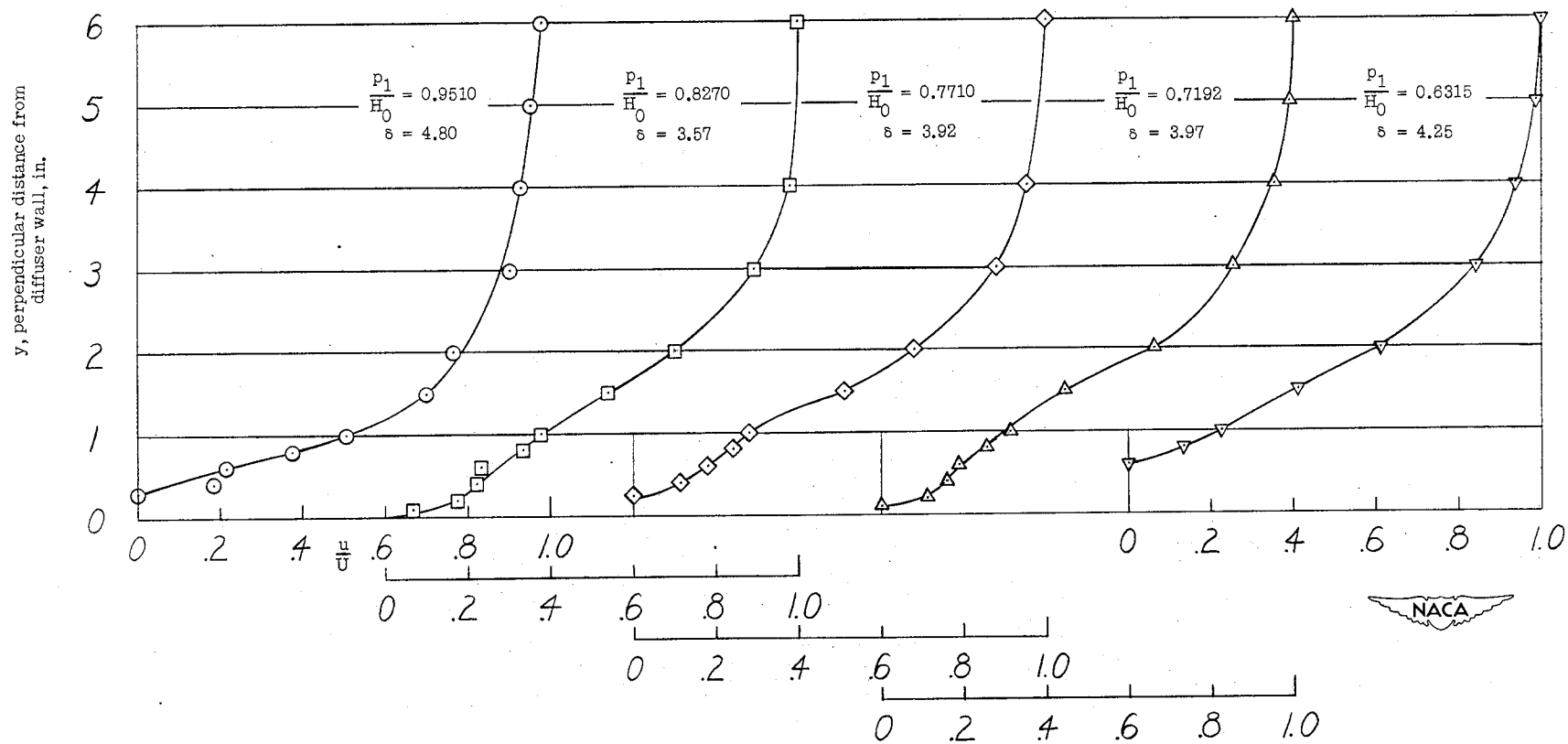
(d) Station 4.

Figure 12.- Continued.
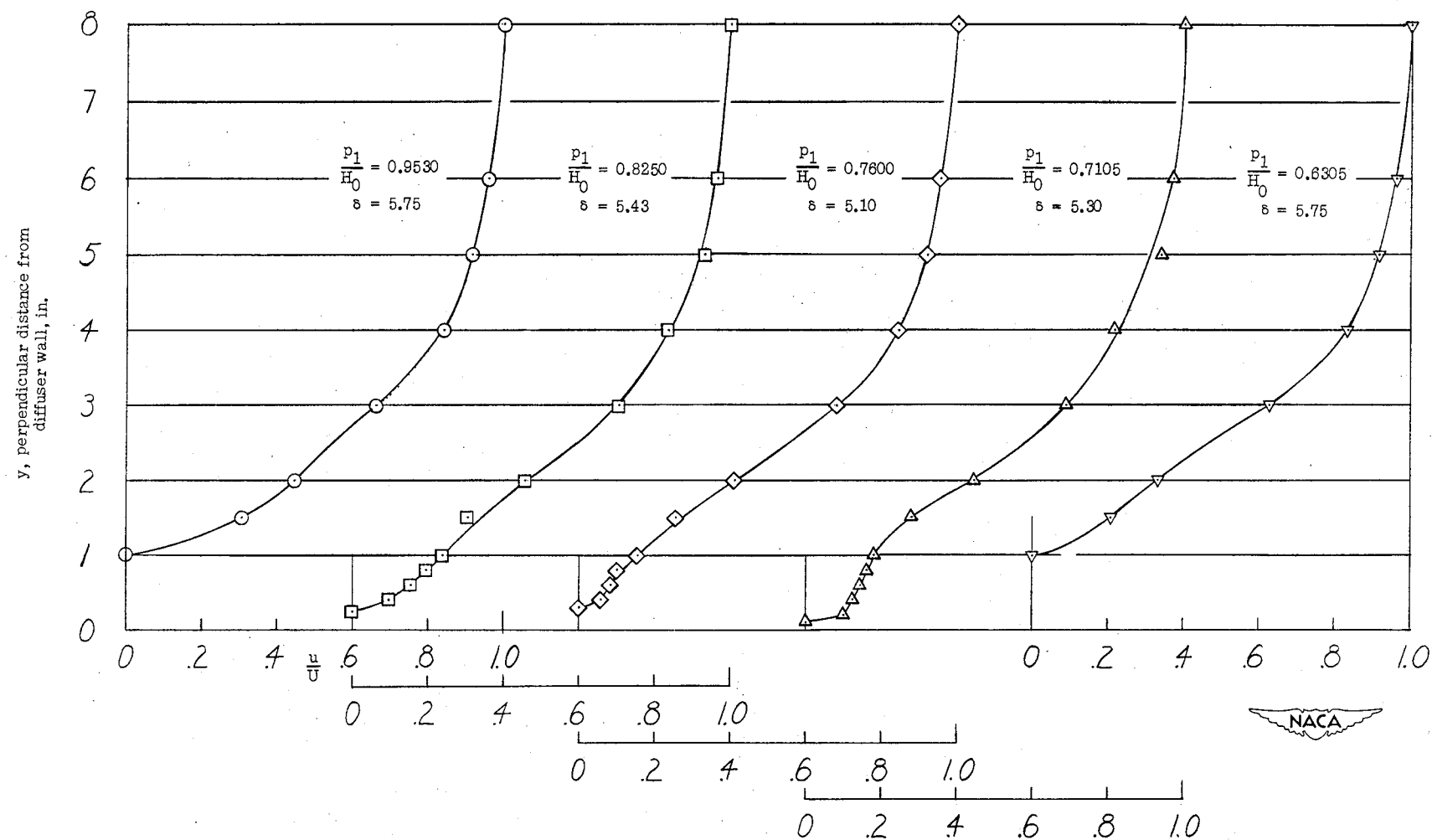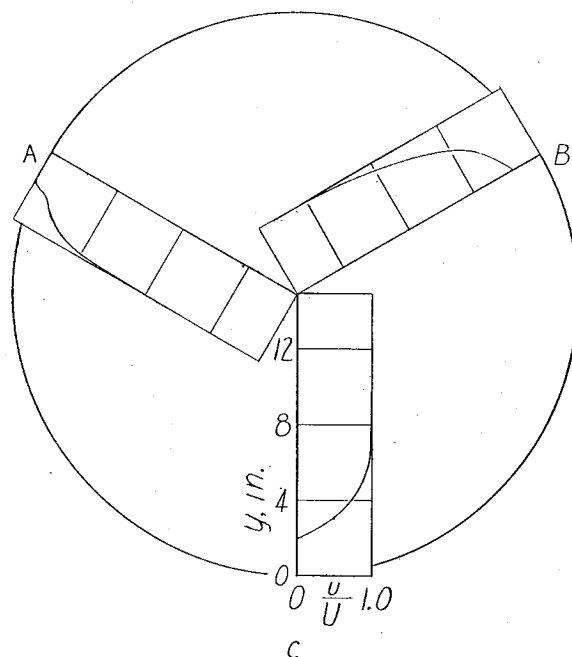
(e) Station 5.

Figure 12.- Continued.

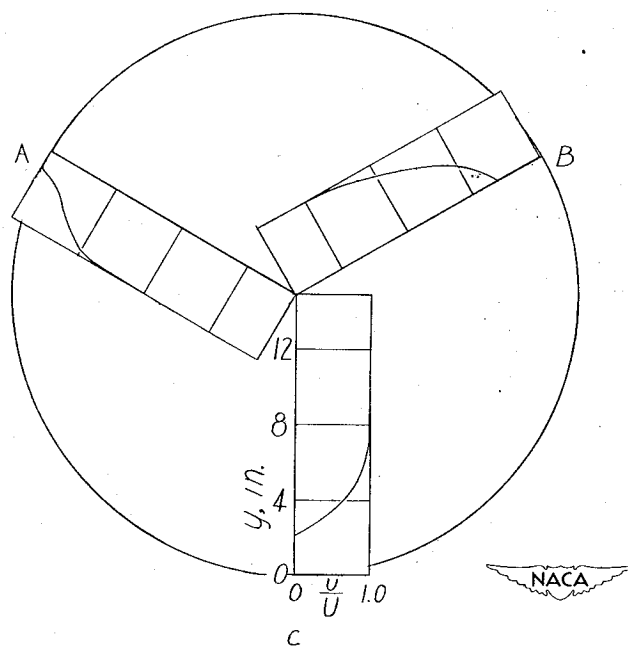y, perpendicular distance from diffuser wall, in.
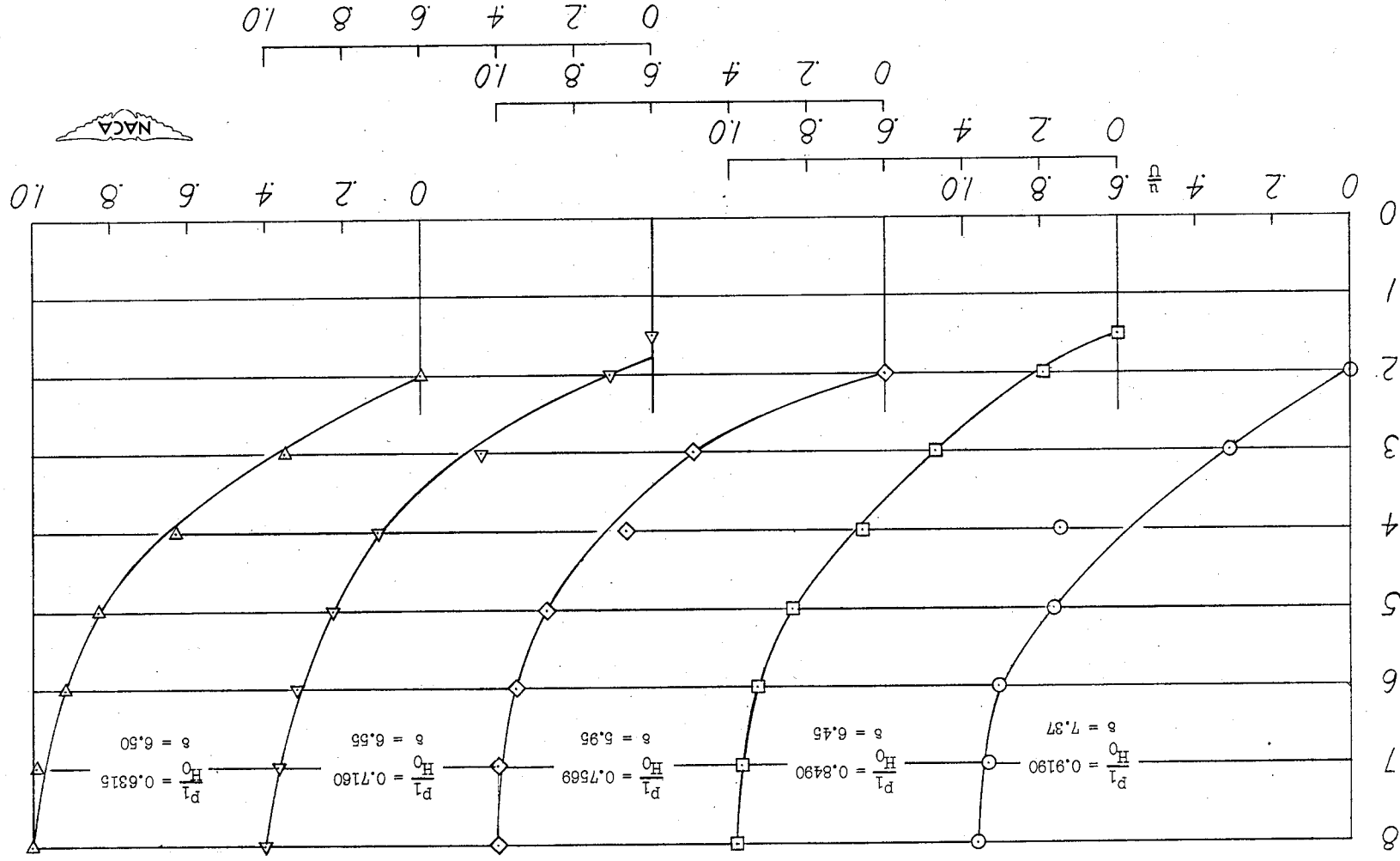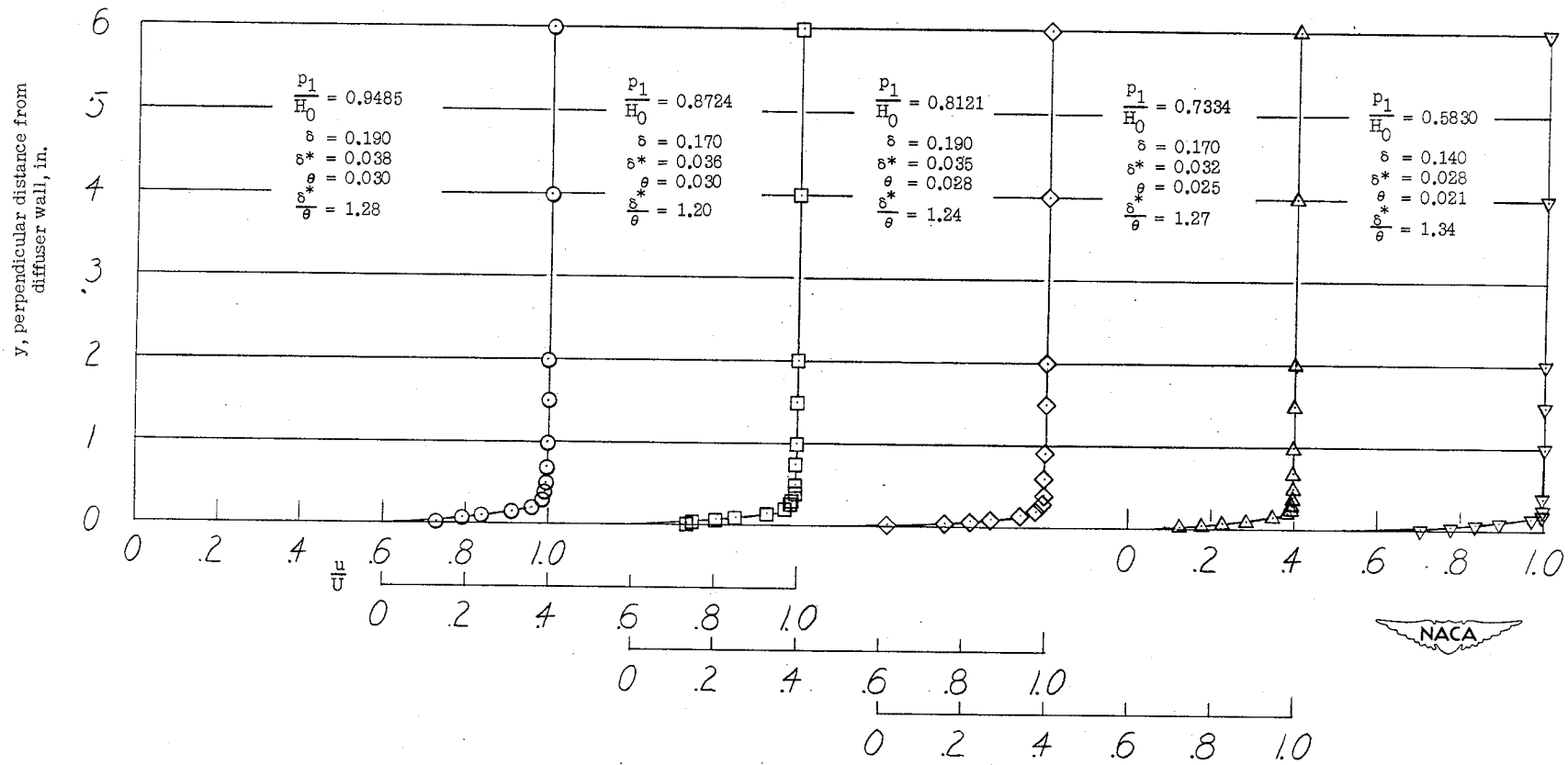

(f) Station 6.

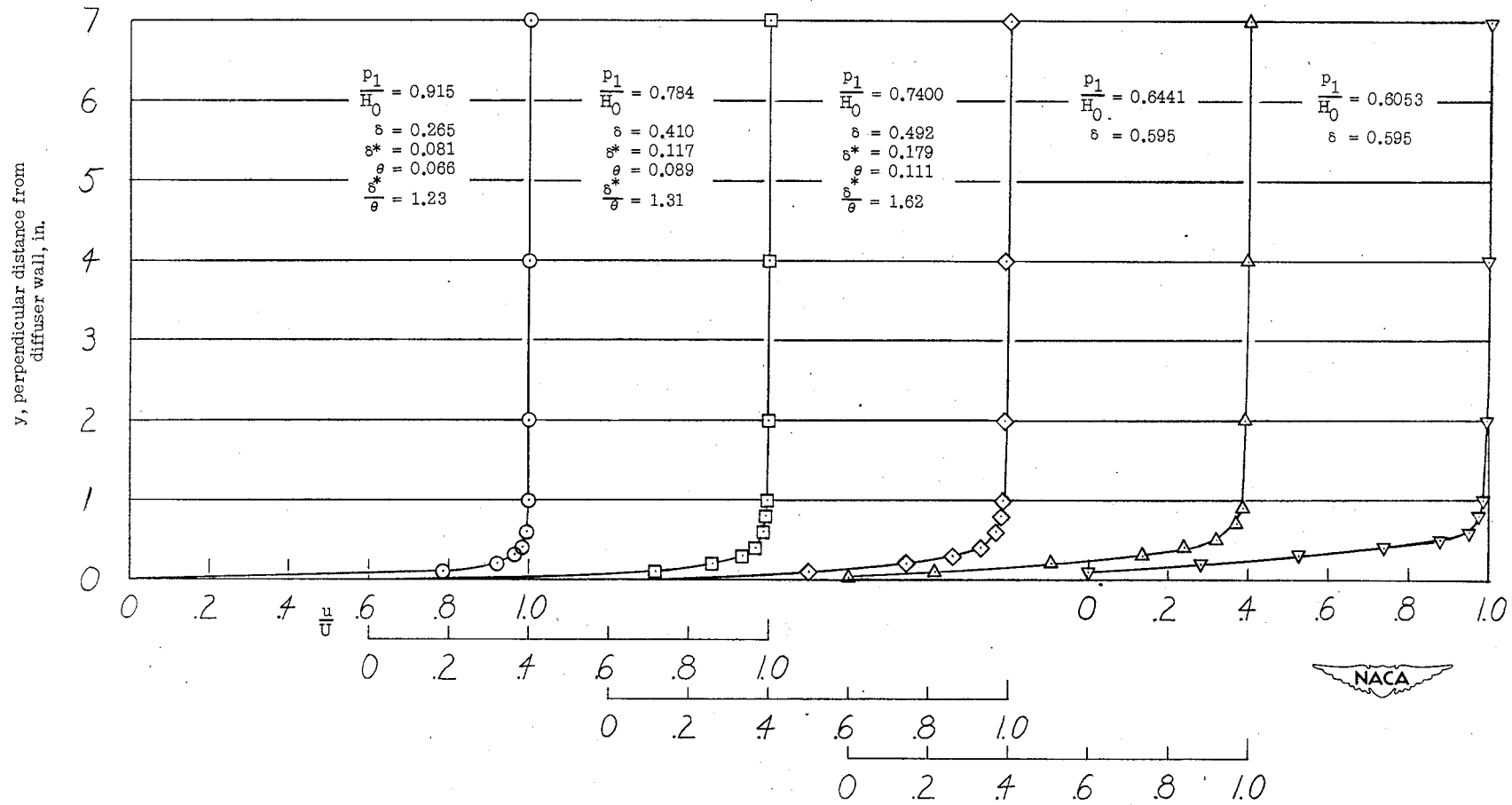Figure 12.- Concluded.

(a) $\dfrac{p_1}{H_0} \approx 0.780.$

(b) $\dfrac{p_1}{H_0} \approx 0.640.$

Figure 13.- Boundary-layer velocity profiles at diffuser exit, station 6.
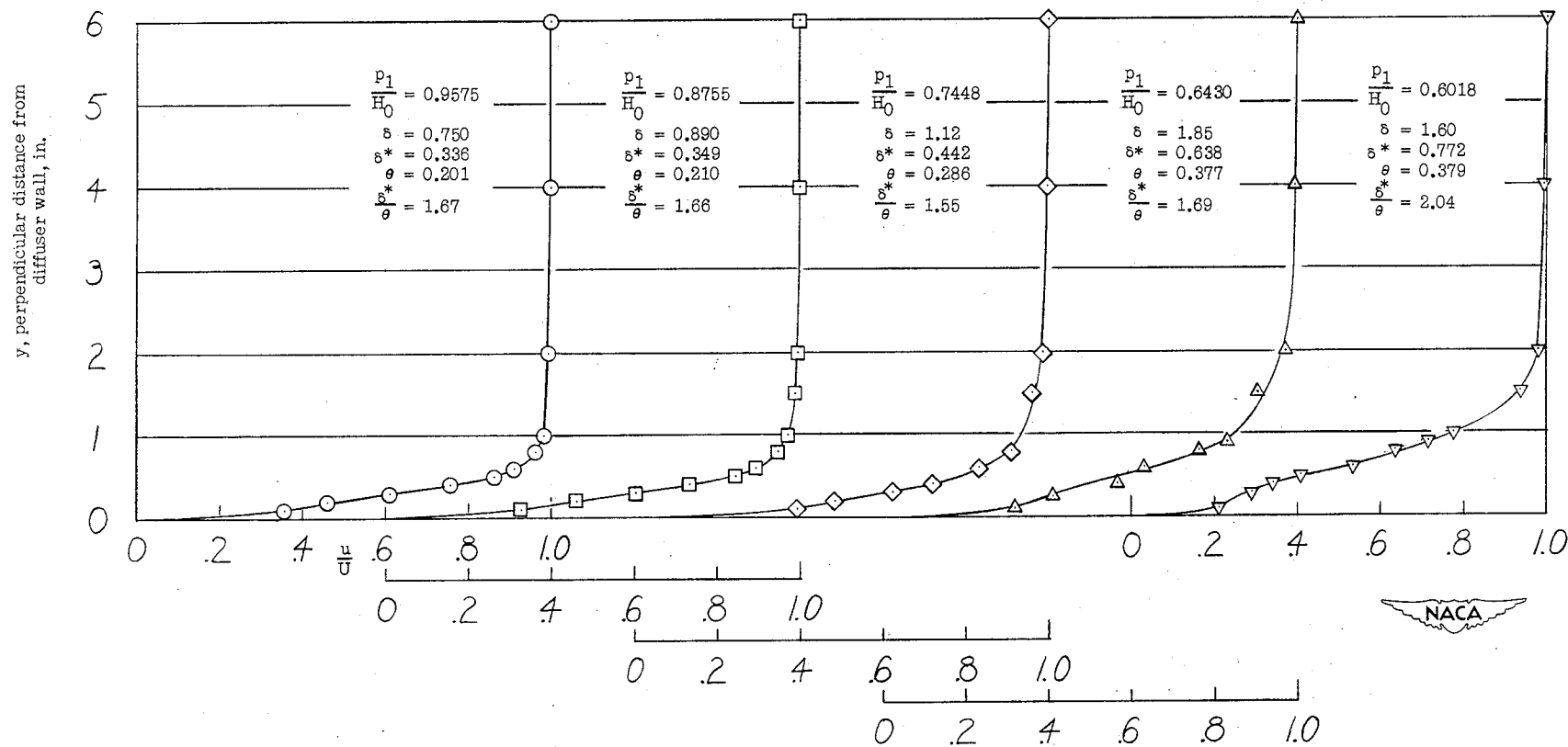Thicker inlet boundary layer.

(a) Station 1.

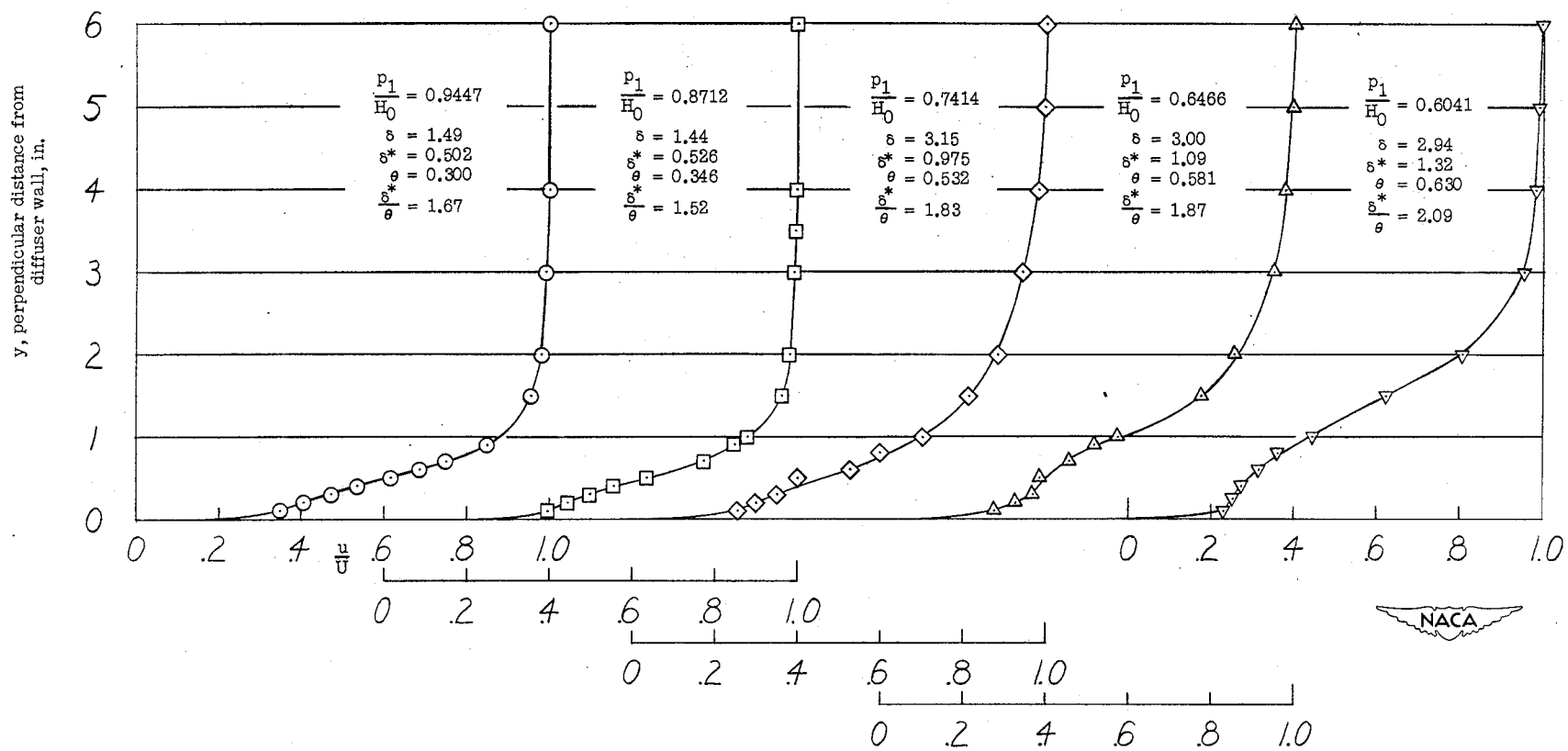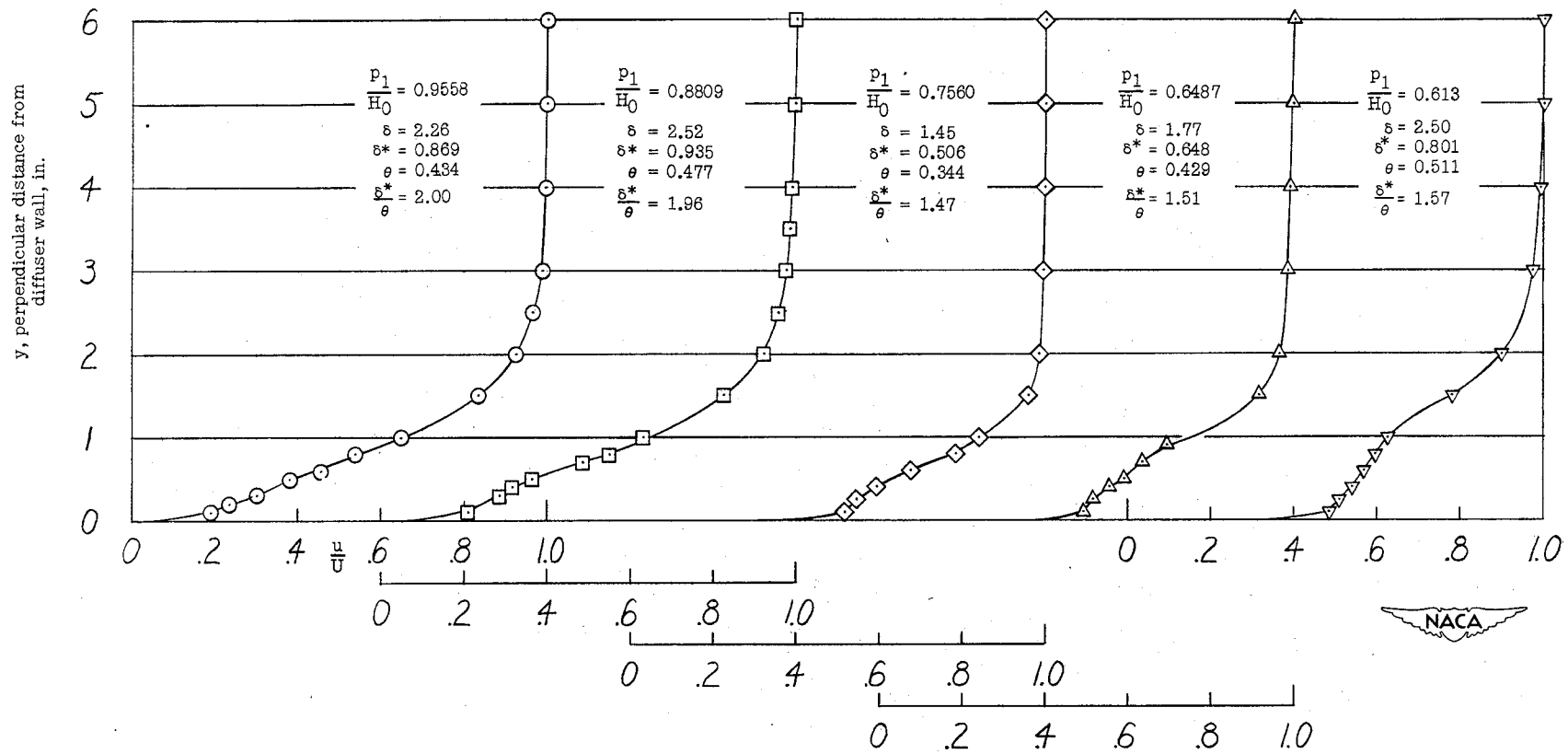Figure 14.- Boundary-layer velocity profiles. Thinner inlet boundary layer.

y, perpendicular distance from diffuser wall, in.

$\frac{p_1}{H_0} = 0.915$

$\delta = 0.265$
$\delta^* = 0.081$
$\theta = 0.066$
$\frac{\delta^*}{\theta} = 1.23$

$\frac{p_1}{H_0} = 0.784$

$\delta = 0.410$
$\delta^* = 0.117$
$\theta = 0.089$
$\frac{\delta^*}{\theta} = 1.31$

$\frac{p_1}{H_0} = 0.7400$

$\delta = 0.492$
$\delta^* = 0.179$
$\theta = 0.111$
$\frac{\delta^*}{\theta} = 1.62$

$\frac{p_1}{H_0} = 0.6441$

$\delta = 0.595$

$\frac{p_1}{H_0} = 0.6053$

$\delta = 0.595$

$\frac{u}{U}$

NACA

(b) Station 2.
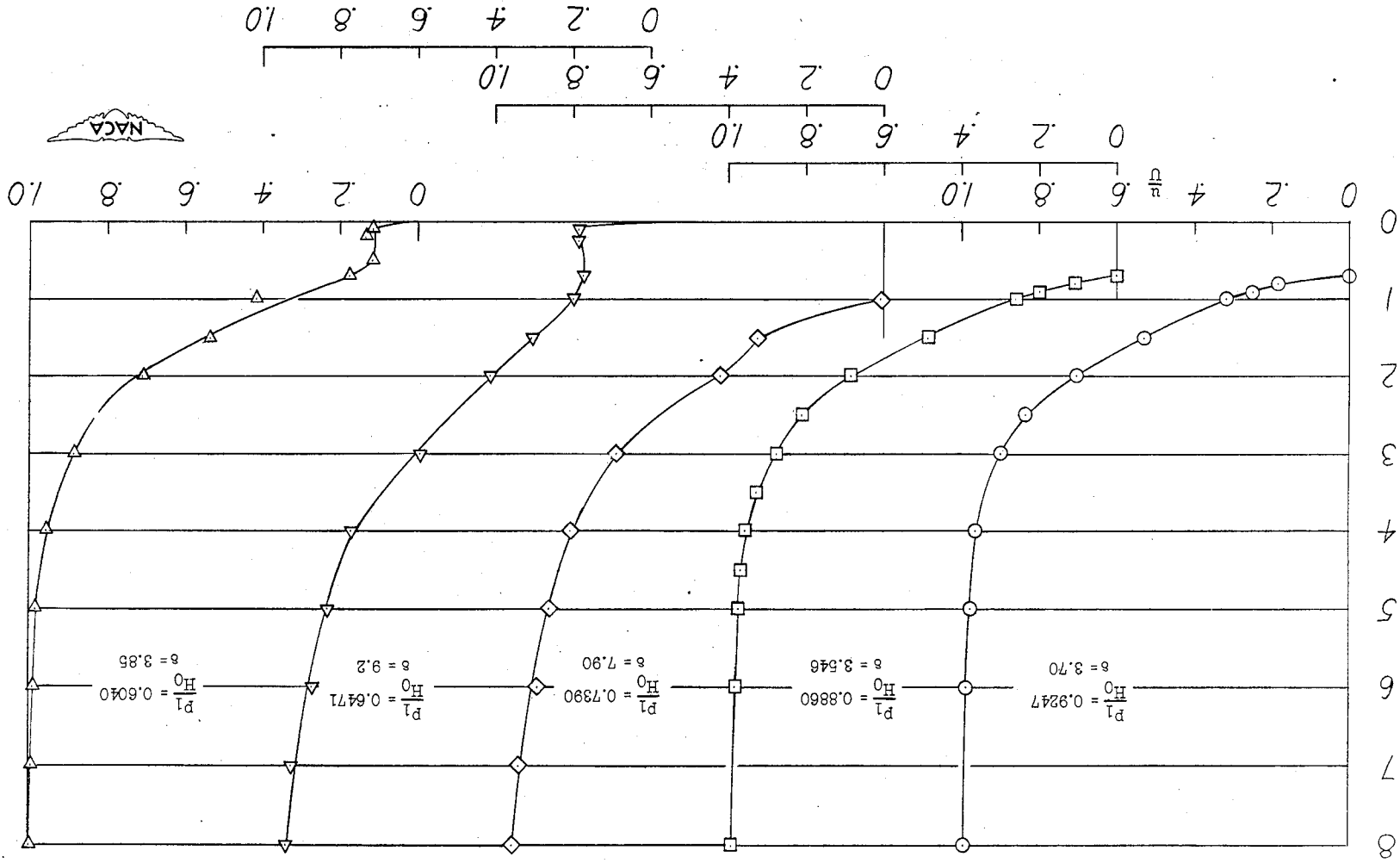
Figure 14.- Continued.

(c) Station 3.

Figure 14.- Continued.

y, perpendicular distance from diffuser wall, in.

$\frac{p_1}{H_0} = 0.9447$

$\delta = 1.49$
$\delta^* = 0.502$
$\theta = 0.300$
$\frac{\delta^*}{\theta} = 1.67$

$\frac{p_1}{H_0} = 0.8712$

$\delta = 1.44$
$\delta^* = 0.526$
$\theta = 0.346$
$\frac{\delta^*}{\theta} = 1.52$

$\frac{p_1}{H_0} = 0.7414$

$\delta = 3.15$
$\delta^* = 0.975$
$\theta = 0.532$
$\frac{\delta^*}{\theta} = 1.83$

$\frac{p_1}{H_0} = 0.6466$

$\delta = 3.00$
$\delta^* = 1.09$
$\theta = 0.581$
$\frac{\delta^*}{\theta} = 1.87$

$\frac{p_1}{H_0} = 0.6041$

$\delta = 2.94$
$\delta^* = 1.32$
$\theta = 0.630$
$\frac{\delta^*}{\theta} = 2.09$

NACA

(d) Station 4.

Figure 14.- Continued.

y, perpendicular distance from
diffuser wall, in.

$$\frac{p_1}{H_0} = 0.9558$$

$\delta = 2.26$
$\delta* = 0.869$
$\theta = 0.434$

$$\frac{\delta*}{\theta} = 2.00$$

$$\frac{p_1}{H_0} = 0.8809$$

$\delta = 2.52$
$\delta* = 0.935$
$\theta = 0.477$

$$\frac{\delta*}{\theta} = 1.96$$

$$\frac{p_1}{H_0} = 0.7560$$

$\delta = 1.45$
$\delta* = 0.506$
$\theta = 0.344$

$$\frac{\delta*}{\theta} = 1.47$$

$$\frac{p_1}{H_0} = 0.6487$$

$\delta = 1.77$
$\delta* = 0.648$
$\theta = 0.429$

$$\frac{\delta*}{\theta} = 1.51$$

$$\frac{p_1}{H_0} = 0.613$$

$\delta = 2.50$
$\delta* = 0.801$
$\theta = 0.511$

$$\frac{\delta*}{\theta} = 1.57$$

$\frac{u}{U}$

NACA

(e) Station 5.

Figure 14.- Continued.

(f) Station 6.

Figure 14.- Concluded.
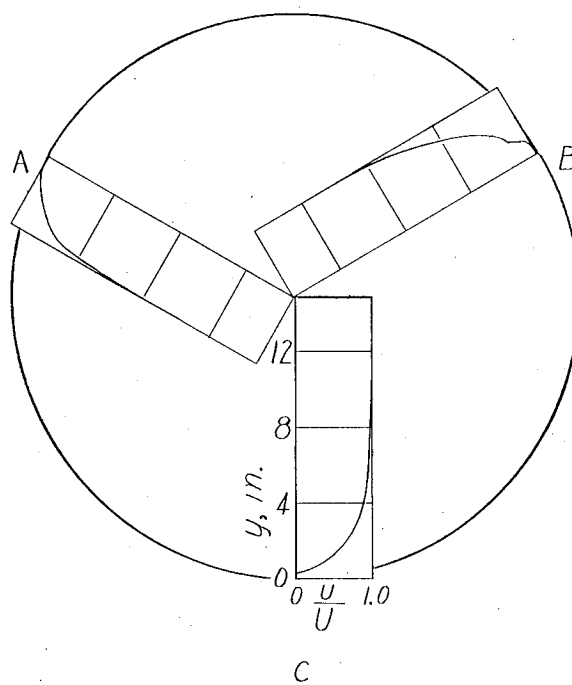
(a) $\dfrac{p_1}{H_0} \approx 0.780.$
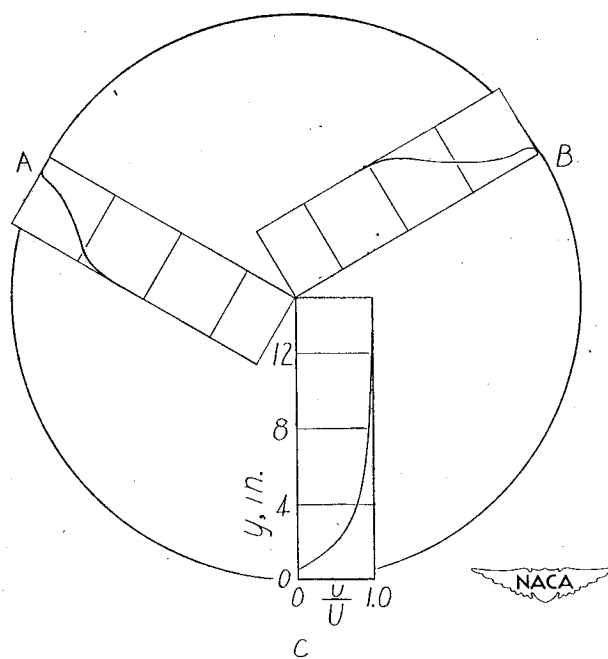
(b) $\dfrac{p_1}{H_0} \approx 0.640.$

Figure 15.- Boundary-layer velocity profiles at diffuser exit, station
Thinner inlet boundary layer.
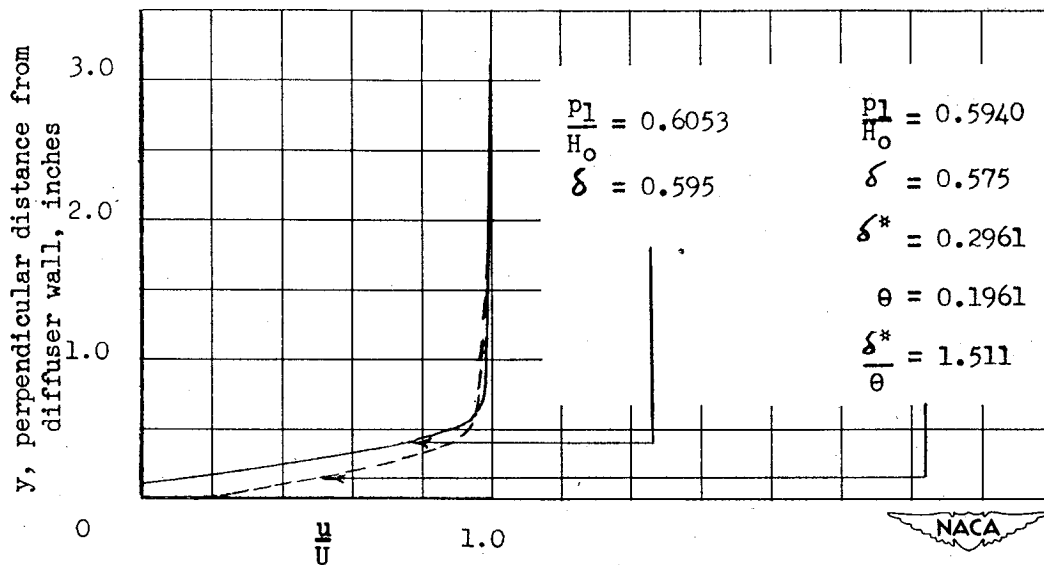
Figure 16.- Boundary-layer velocity profiles at station 2 showing
separated and unseparated flow at approximately the same inlet
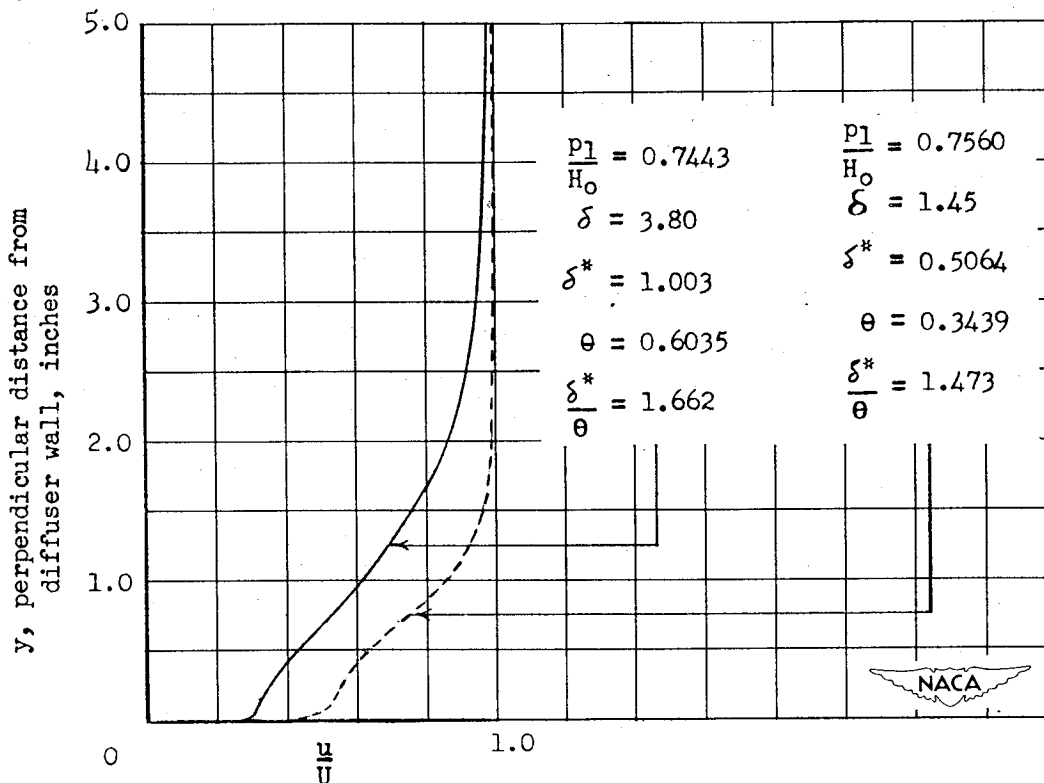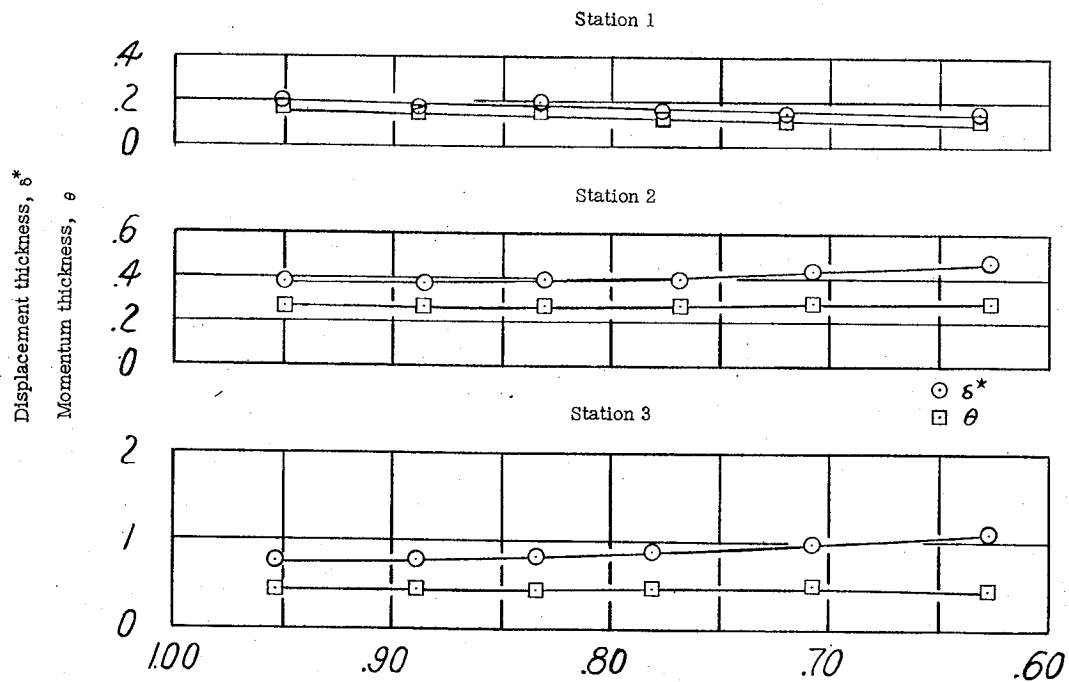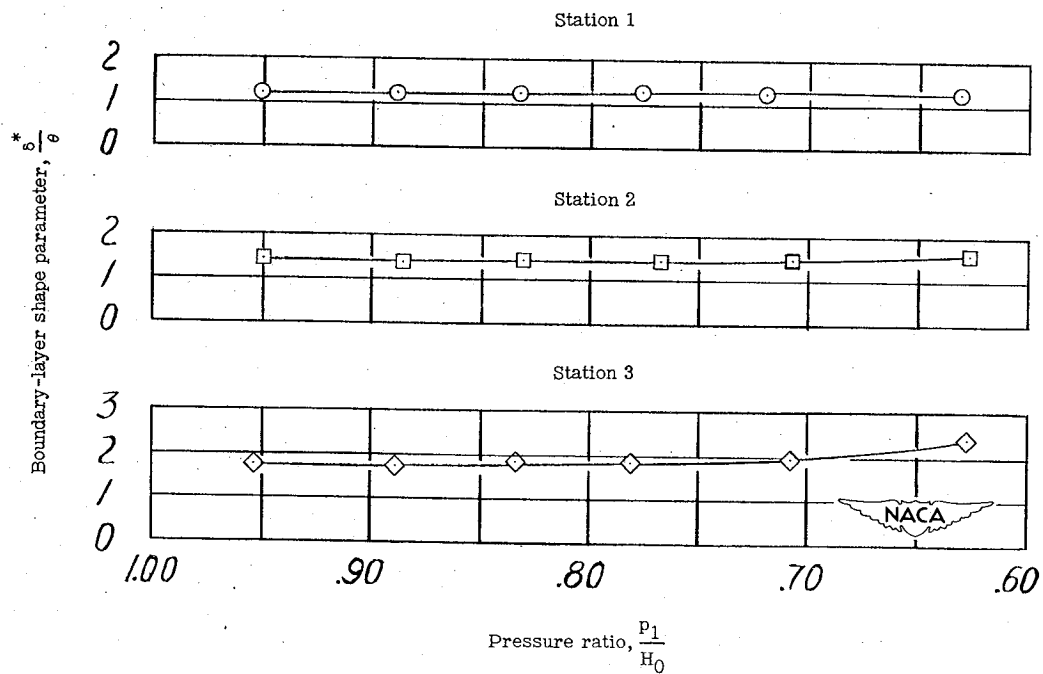velocity. Thinner inlet boundary layer.

Figure 17.- Boundary-layer velocity profiles at station 5 showing
different shapes at approximately the same inlet velocity.
Thinner inlet boundary layer.

(a) Variation of displacement thickness and momentum thickness.

(b) Variation of boundary-layer shape parameter.

Figure 18.- Variation of boundary-layer parameters with inlet pressure
ratio. Thicker inlet boundary layer.
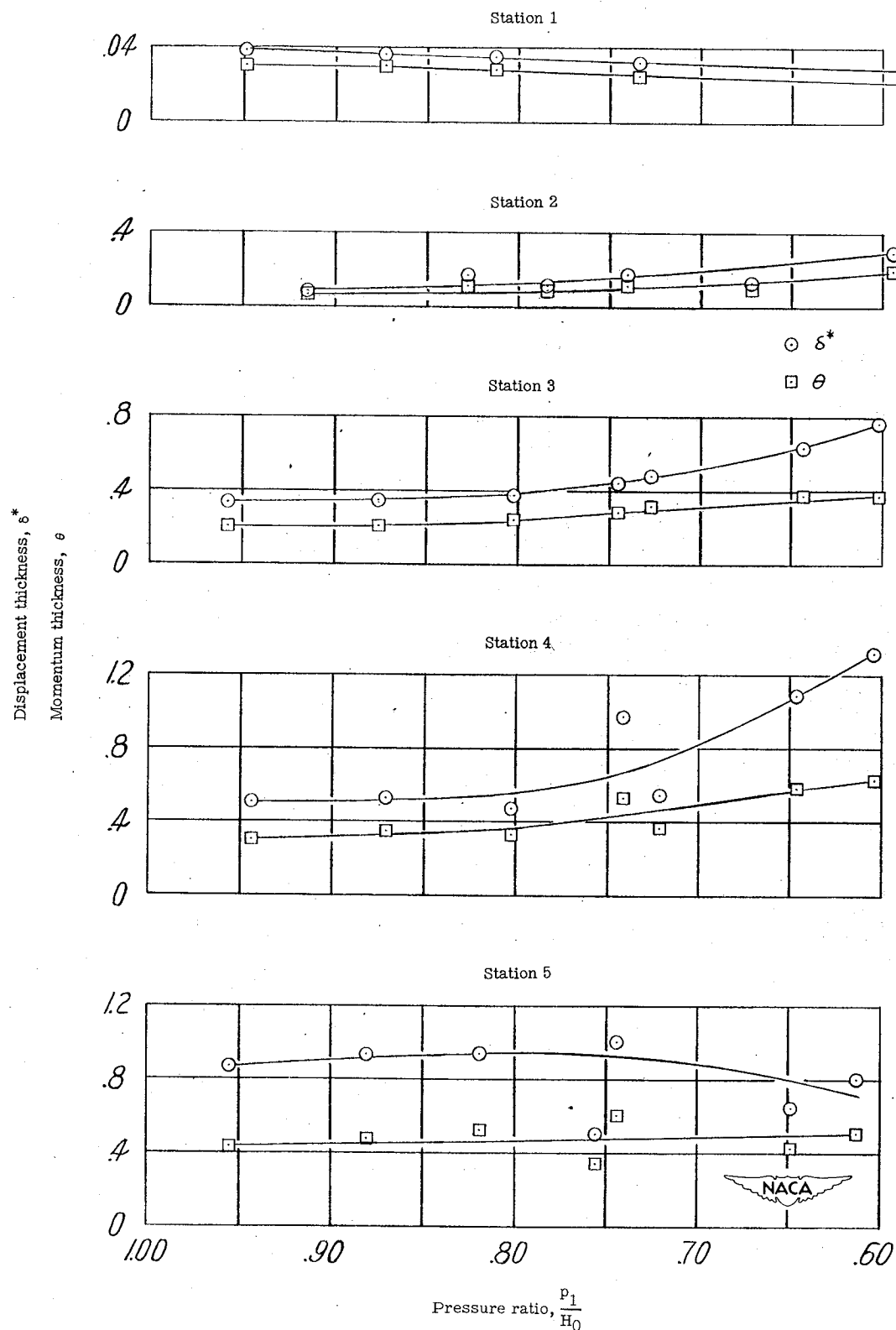
Figure 19.- Variation of displacement thickness and momentum thickness
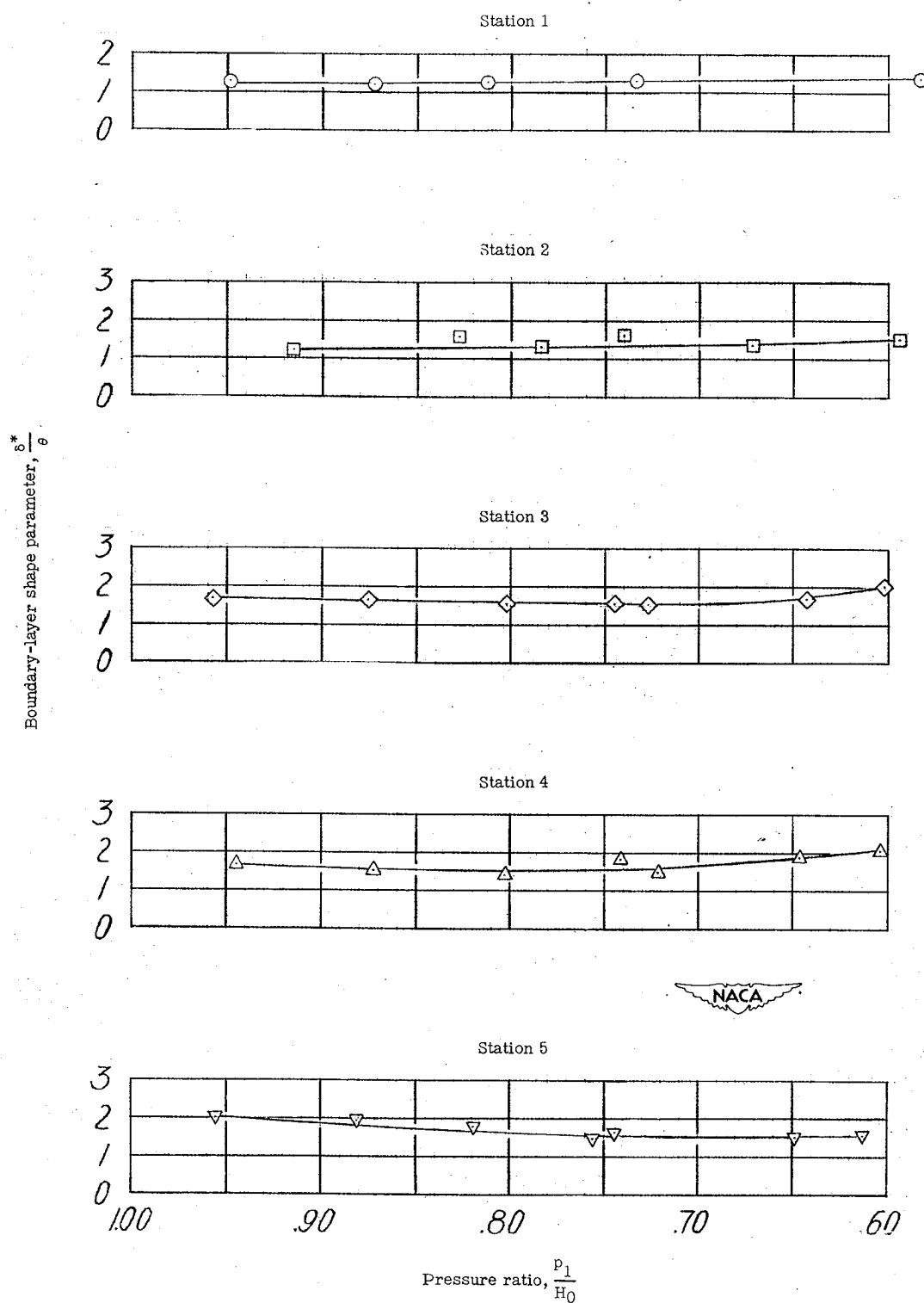with inlet pressure ratio. Thinner inlet boundary layer.

Station 1

Station 2

Station 3

Station 4

Station 5

Boundary-layer shape parameter, $\dfrac{\delta^*}{\theta}$

Pressure ratio, $\dfrac{p_1}{H_0}$

Figure 20.- Variation of boundary-layer shape parameter with inlet
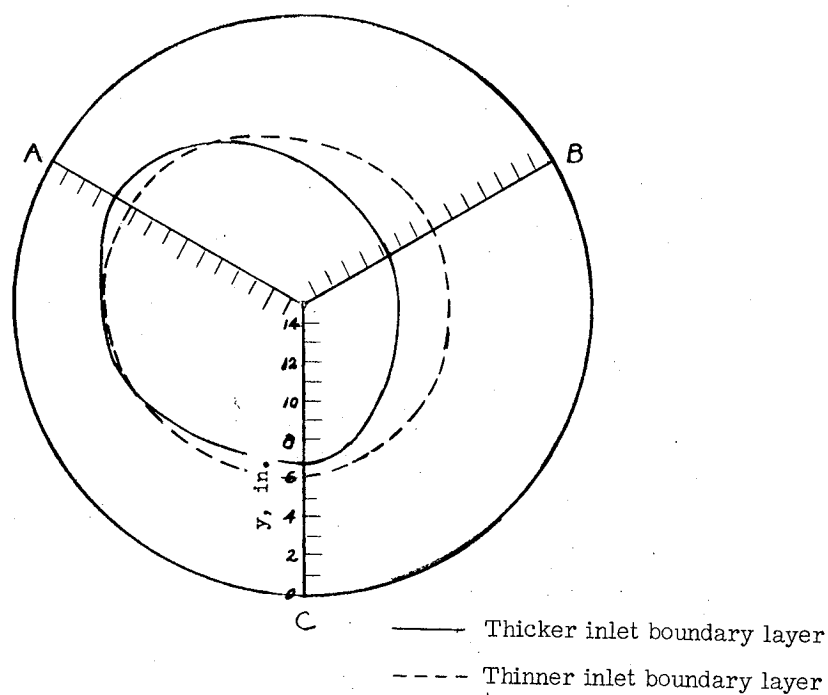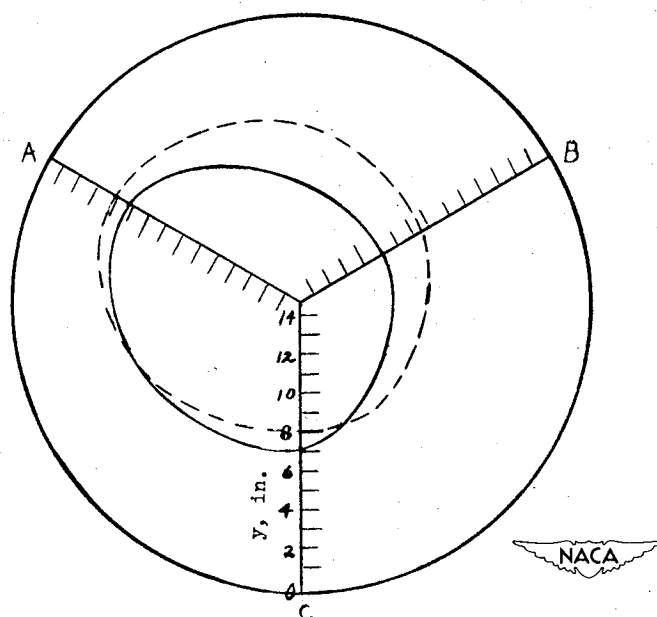pressure ratio. Thinner inlet boundary layer.
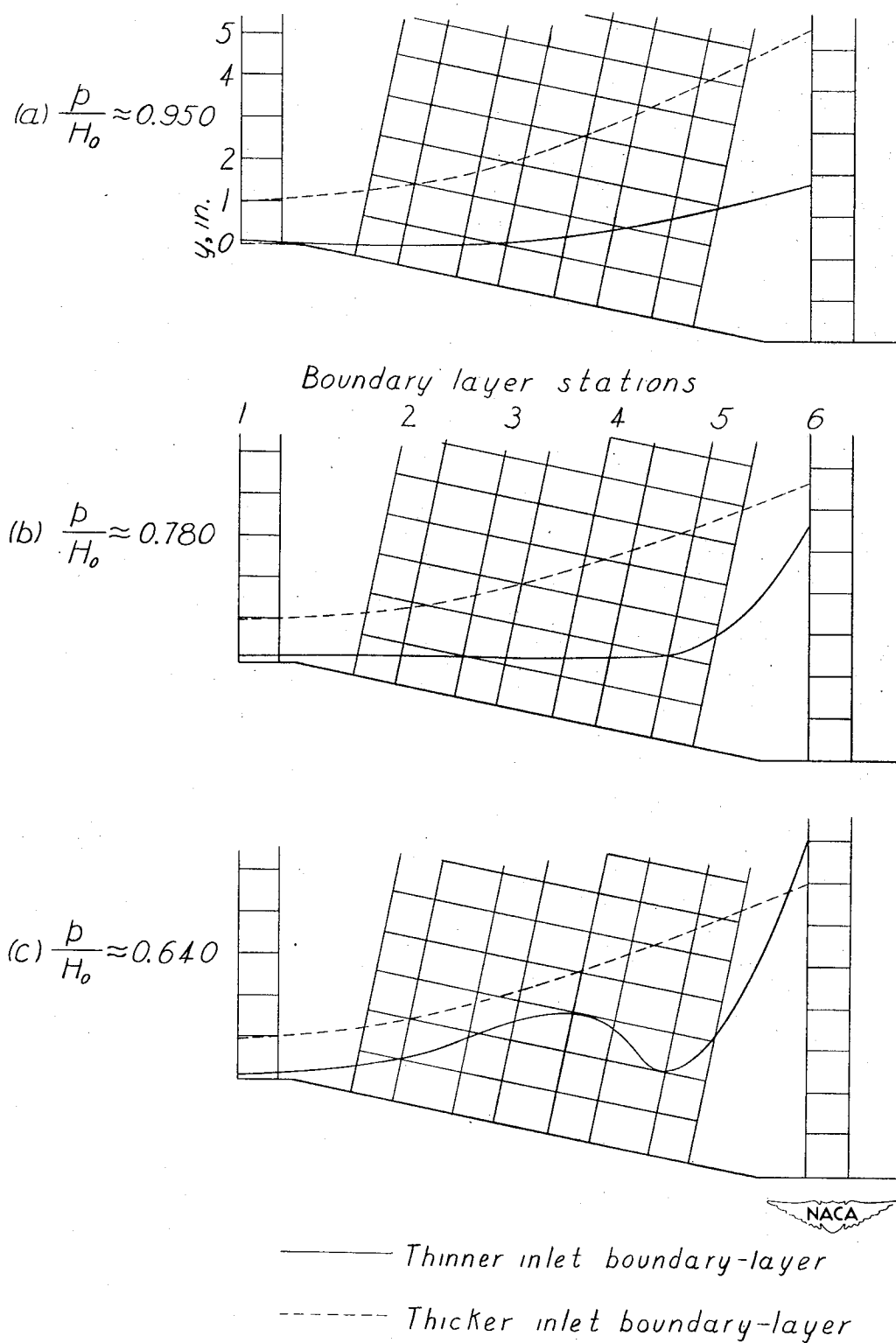
Figure 21.- Development of boundary-layer thickness along wall of diffuser for three inlet velocities. Both inlet boundary-layer thicknesses.

(a) $\dfrac{p_1}{H_0} \approx 0.780$.

(b) $\dfrac{p_1}{H_0} \approx 0.640$.

Figure 22.- Distribution of the boundary-layer thickness at the diffuser
exit, station 6, for two inlet velocities. Both inlet boundary-layer
thicknesses.